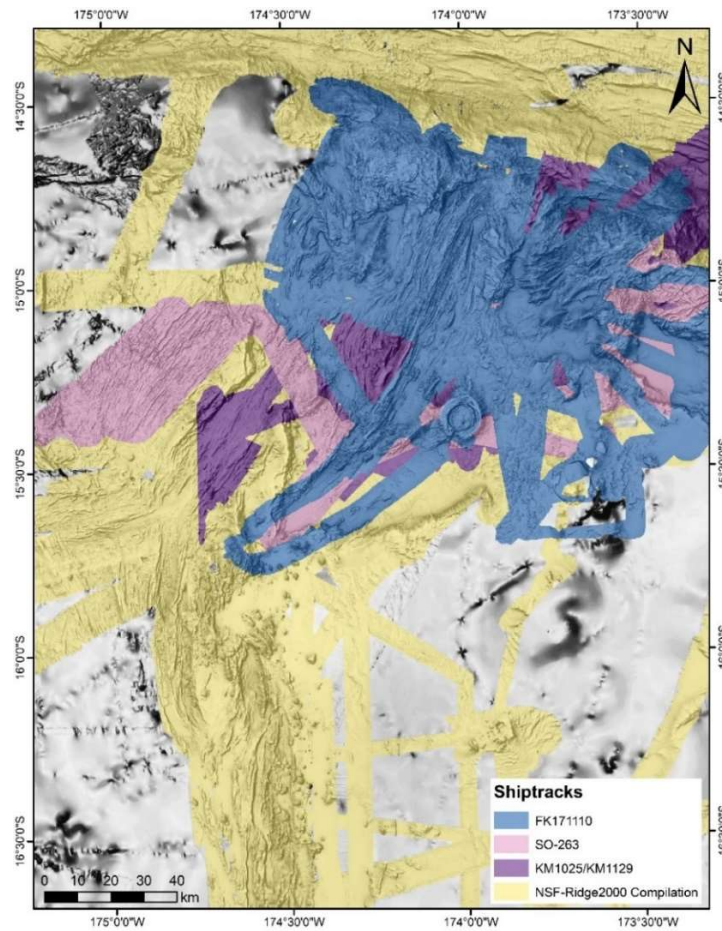


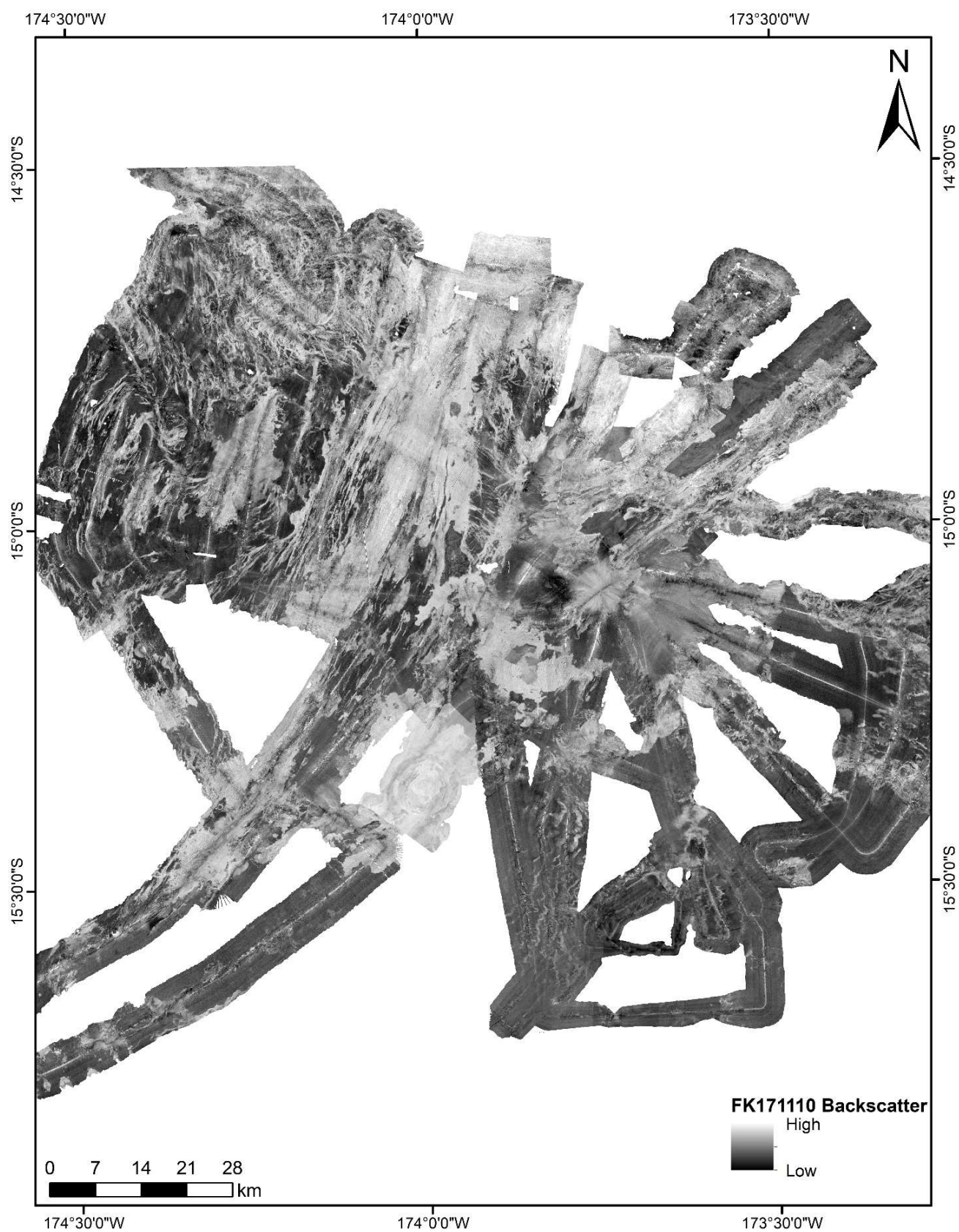
## 1 Supplementary Figures and Tables

Supporting information for this article include data sources for the bathymetric compilation (**Supplementary Figs. S1 and S2**), compiled samples to inform the remote-predictive geological map (**Supplementary Fig. S3**), interpretations of the CMT focal plane solutions (**Supplementary Figs. S4 and S5**), higher-resolution maps of structures (**Supplementary Figs. S6 to S40**), a close-up view of an inferred anticline structure (**Supplementary Fig. S41**), details of the interpreted crustal types (**Supplementary Table S1**), and additional descriptions of the remote-predictive geologic map units (**Supplementary Table S2**).

### 1.1 Supplementary Figures

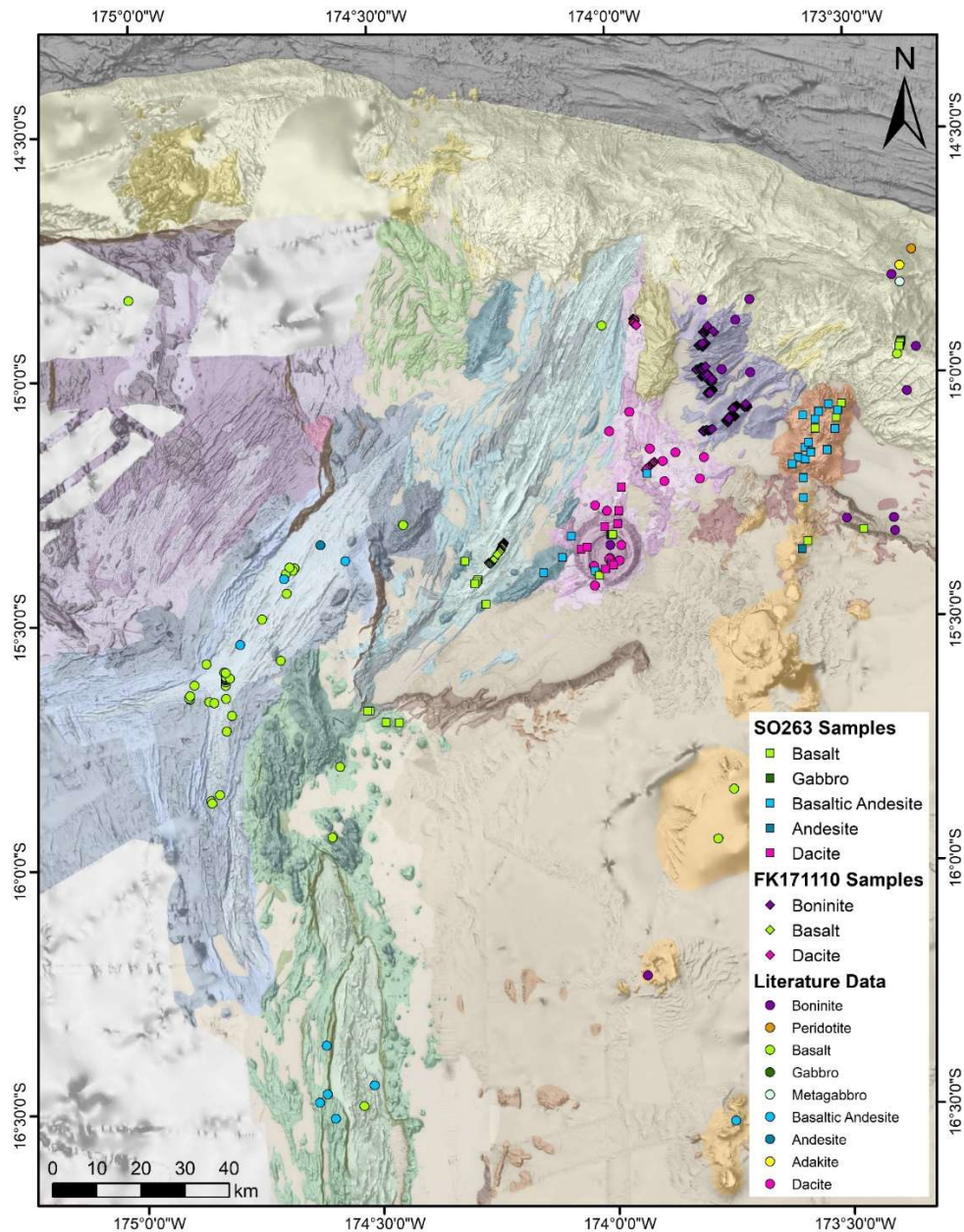


**Supplementary Figure S1.** Compilation of multibeam bathymetry data from FK171110 (25 m resolution) from Merle et al. (2018), SO-263 (30 m resolution) from Haase et al. (2018), KM1025 (50 m resolution) from Rubin et al. (2010) and KM1129 (50 m resolution) from Martinez et al. (2013), and NSF-Ridge2000 (R2K) compilation grid (<50 m resolution) by F. Martinez (Sleeper and Martinez, 2016, and references therein), overlain on the 2019 GEBCO grid (GEBCO Compilation Group, 2019) shown in grey. Mapping in areas shown in grey have a lower degree of confidence than mapping in the areas covered by ship tracks.

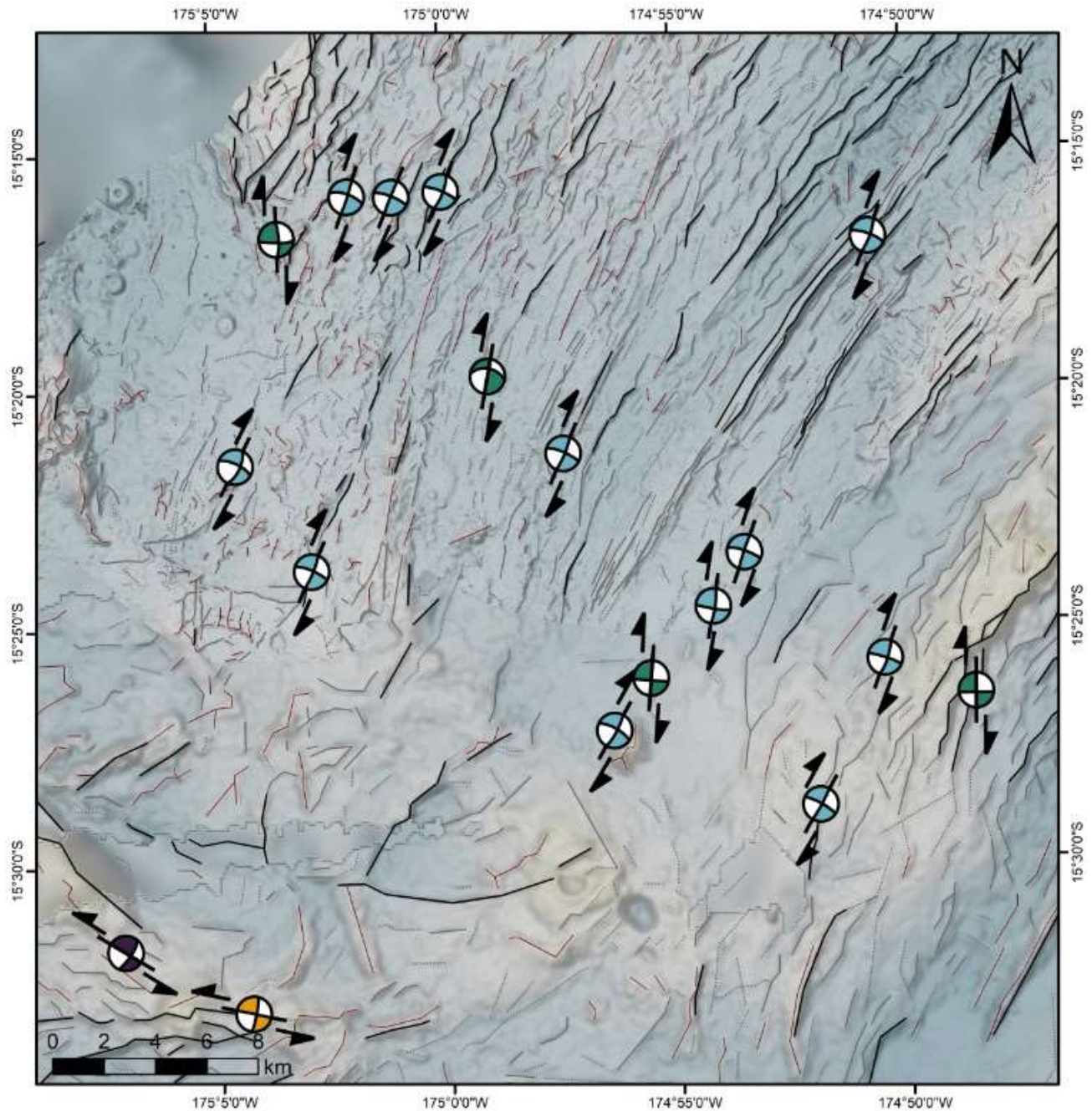


**Supplementary Figure S2.** Backscatter data from the FK171110 cruise from Merle et al. (2018).



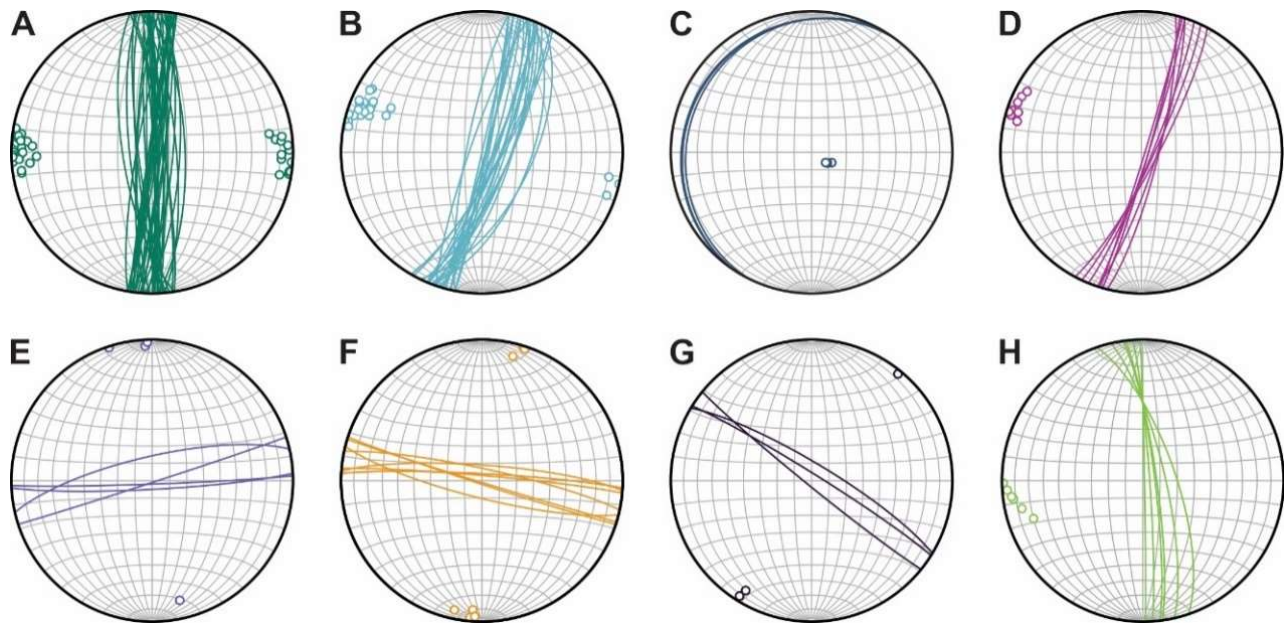


**Supplementary Figure S3.** Compilation of seafloor sample lithologies from FK171110 from Rubin et al. (2018), and SO-263 from Haase et al. (2018), and literature data, including Falloon et al. (1987), Volpe et al. (1988), Sunkel (1990), Looock et al. (1990), Falloon and Crawford (1991), Falloon et al. (1992), Poreda and Craig (1992), Danyushevsky et al. (1993), Hilton et al. (1993), Honda et al. (1993), Dril et al. (1997), Ewart et al. (1998), Sun et al. (2003), Turner et al. (2006), Falloon et al. (2007), Keller et al. (2008), Layne et al. (2009), Lupton et al. (2009), Tian et al. (2011), Dale et al. (2012), Hahm et al. (2012), Lupton et al. (2012), Lytle et al. (2012), Meffre et al. (2012), Birner et al. (2017), Nielsen et al. (2017), Brens et al. (2018), Embley and Rubin (2018), Kendrick et al. (2019), Wang et al. (2019), Zhu et al. (2020). These lithologies inform the geological map in **Figure 5** (underlain here al. (2019)).

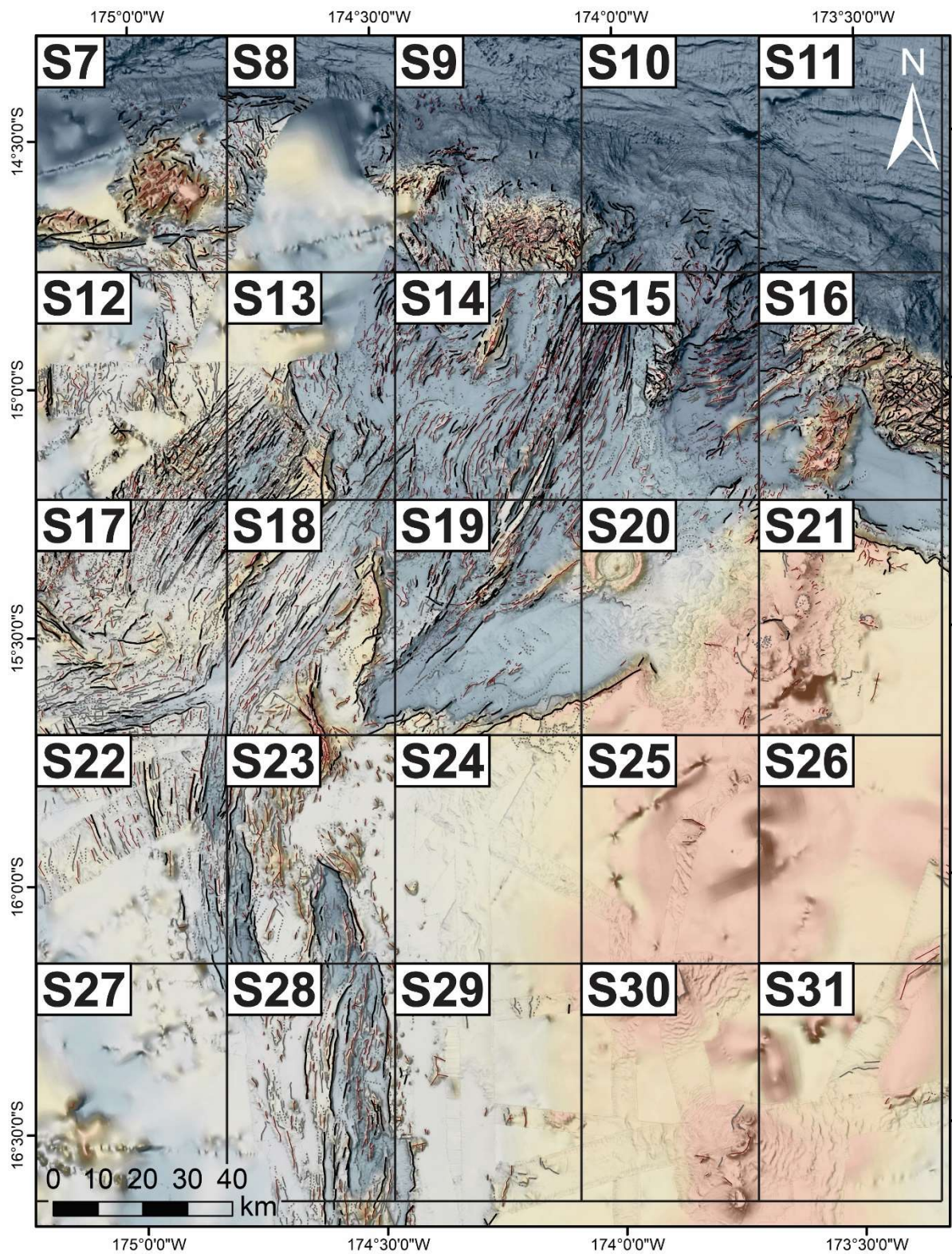


**Supplementary Figure S4.** Example of CMT fault plane solutions based on lineament orientation within the Western Rift Zone assemblage, as shown in **Figure 8**. Dominant lineament fabrics of the surrounding seafloor are used in areas where the CMT is not clearly aligned with a single fault. Here, the dominant fault plane solutions are NNE-trending (light blue), and N-trending solutions (green). In the SW part of the map, E-trending (orange) and WNW-trending (purple) fault-plane solutions are identified.



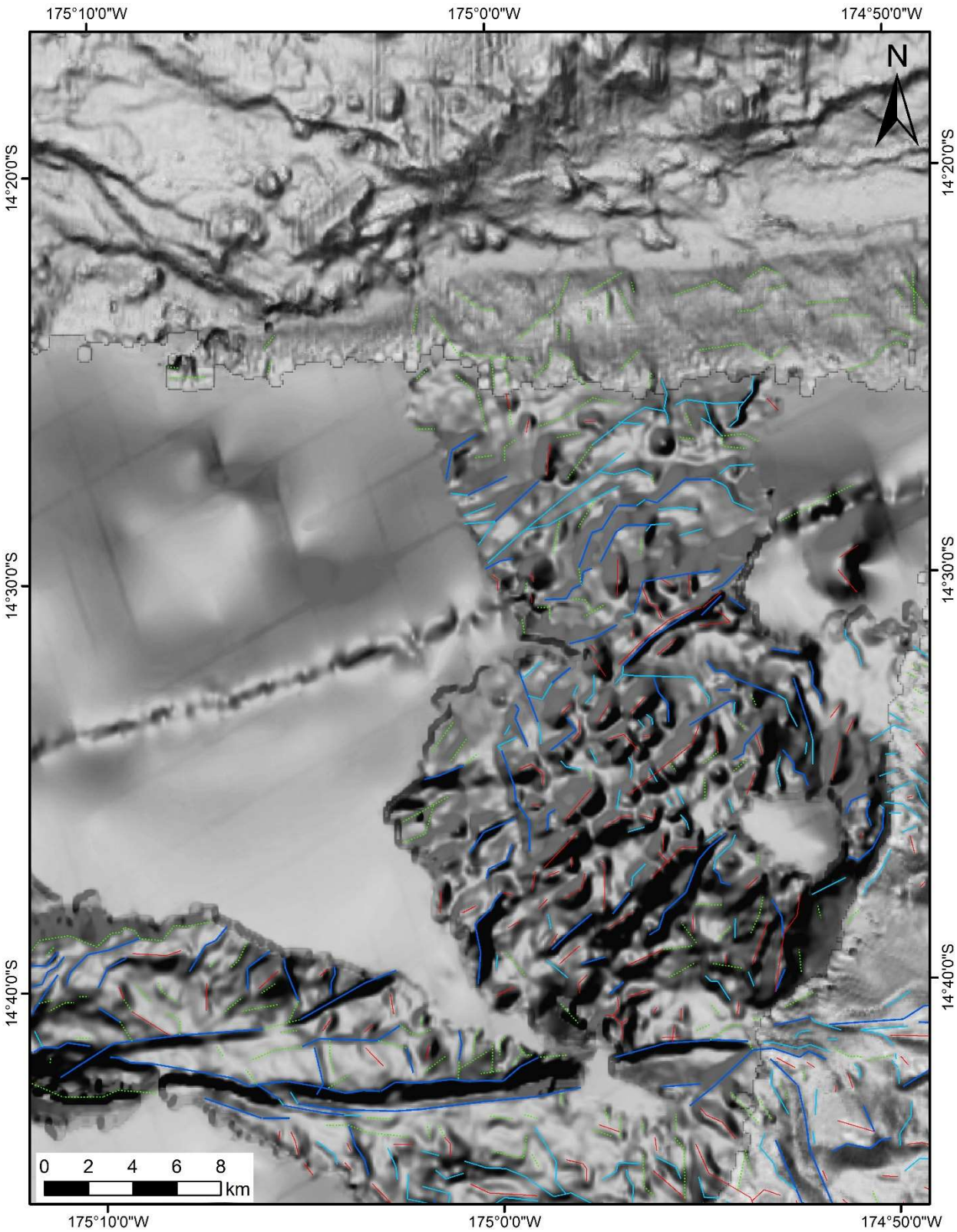


**Supplementary Figure S5.** Stereonets of interpreted CMT fault planes grouped according to orientation: (a) N-trending R-lateral strike-slip, (b) NNE-trending R-lateral strike-slip, (c) NE-trending dip-slip, (d) NNE-trending L-lateral strike-slip, (e) E-trending L-lateral strike-slip, (f) W-trending L-lateral strike-slip, (g) WNW-trending L-lateral strike slip, and (h) NNW-trending L-lateral strike slip.

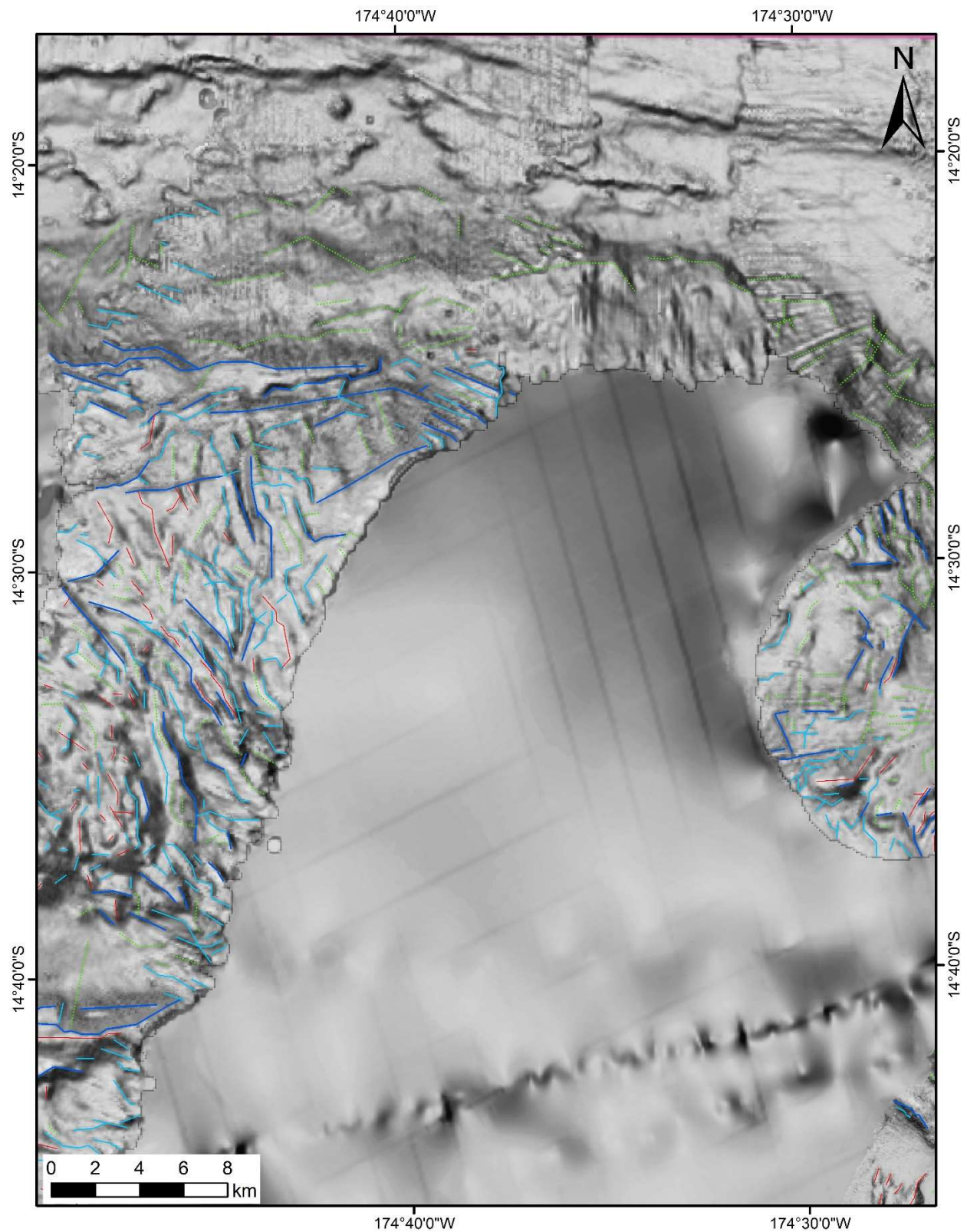




**Supplementary Figure S6.** Overview of the locations of the close-up maps in the following figures (Supplementary Figures S7 to S31) with manually interpreted lineaments overlain on bathymetric data.

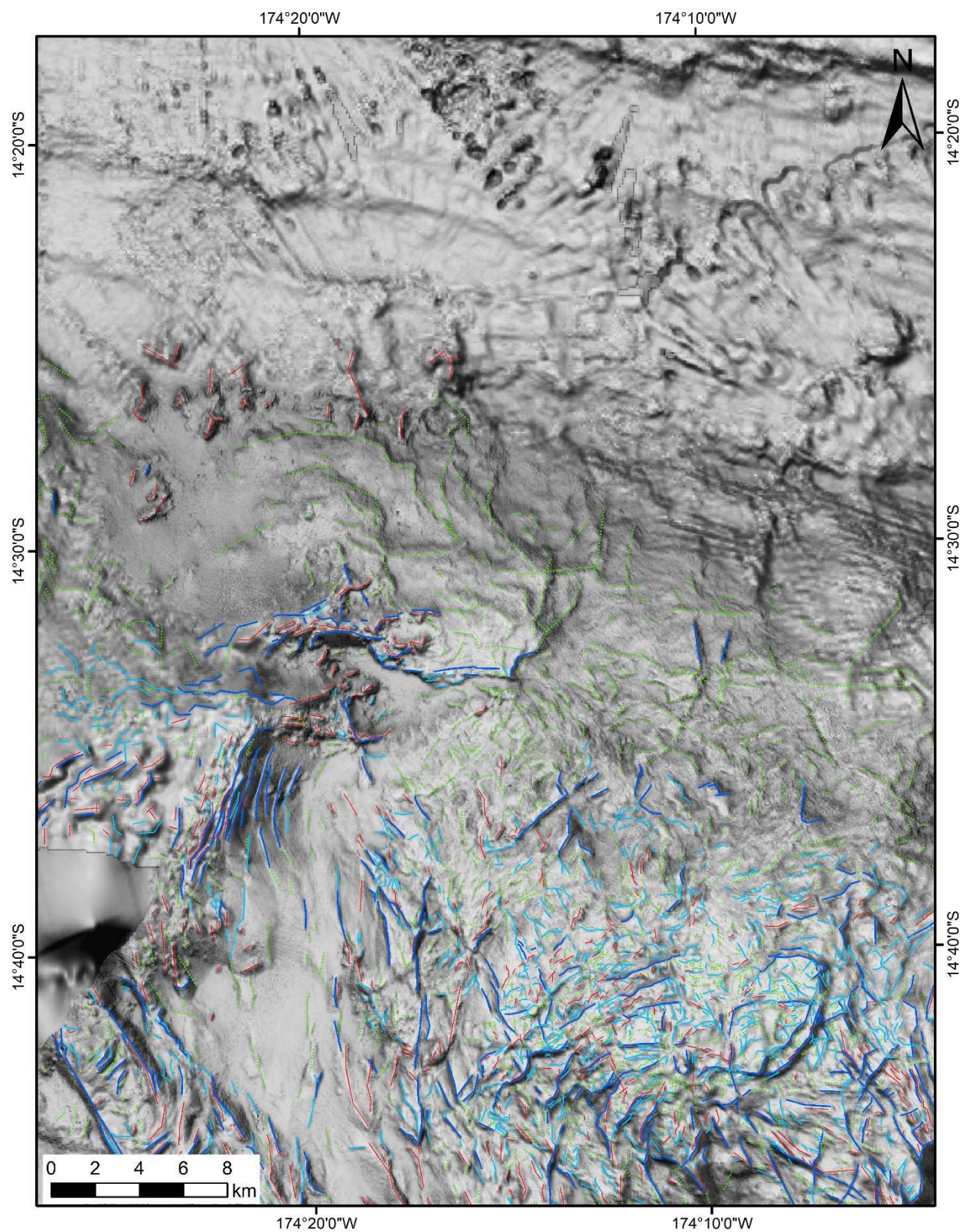


**Supplementary Figure S7.** Close-up of manually interpreted structures overlain on grayscale-shaded bathymetry, with the location shown on **Supplementary Fig. S6**. Major faults are dark blue, minor faults are light blue, volcanic ridges are red, and lineaments are green.



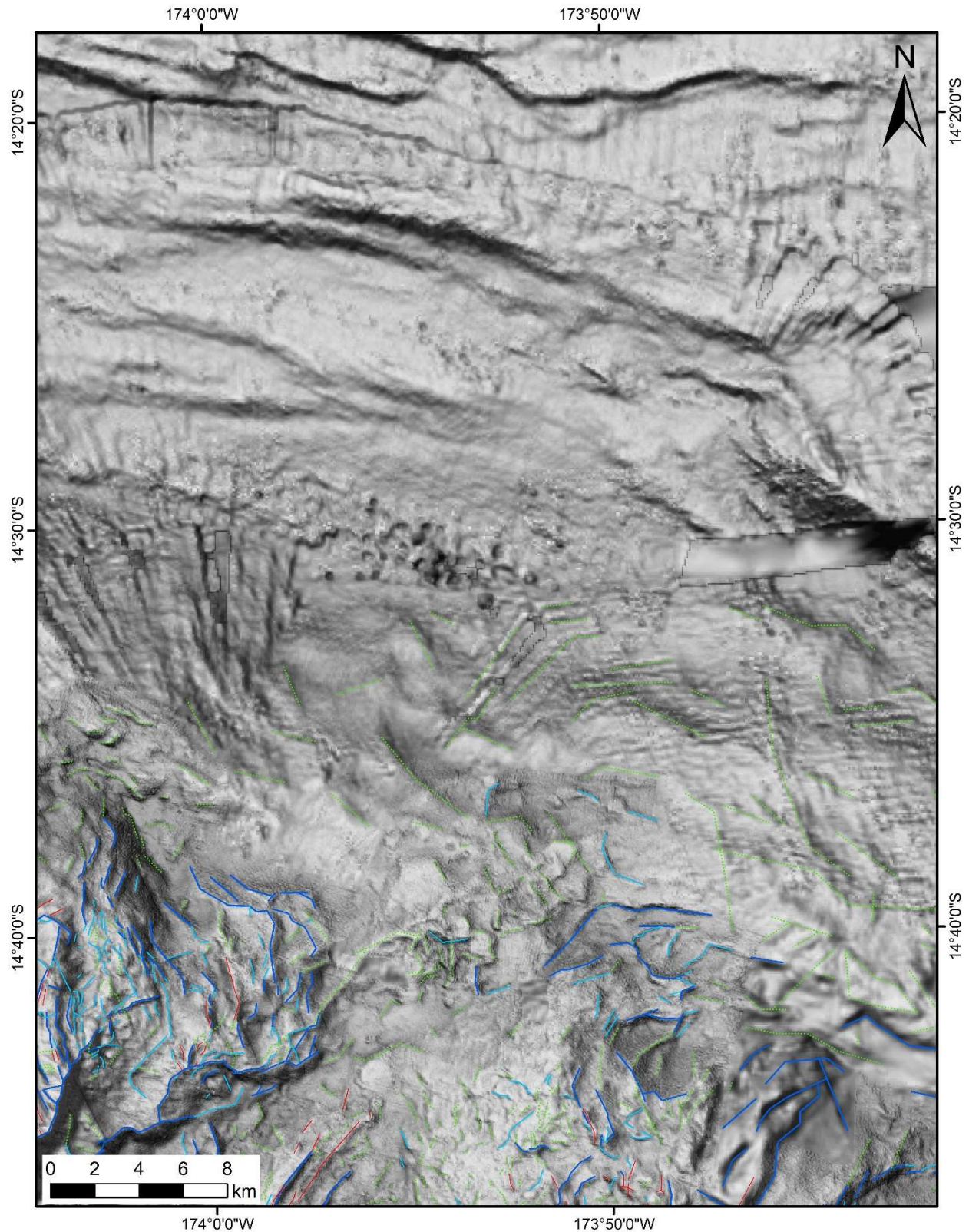


**Supplementary Figure S8.** Close-up of manually interpreted structures overlain on grayscale-shaded bathymetry, with the location shown on **Supplementary Fig. S6**. Major faults are dark blue, minor faults are light blue, volcanic ridges are red, and lineaments are green.



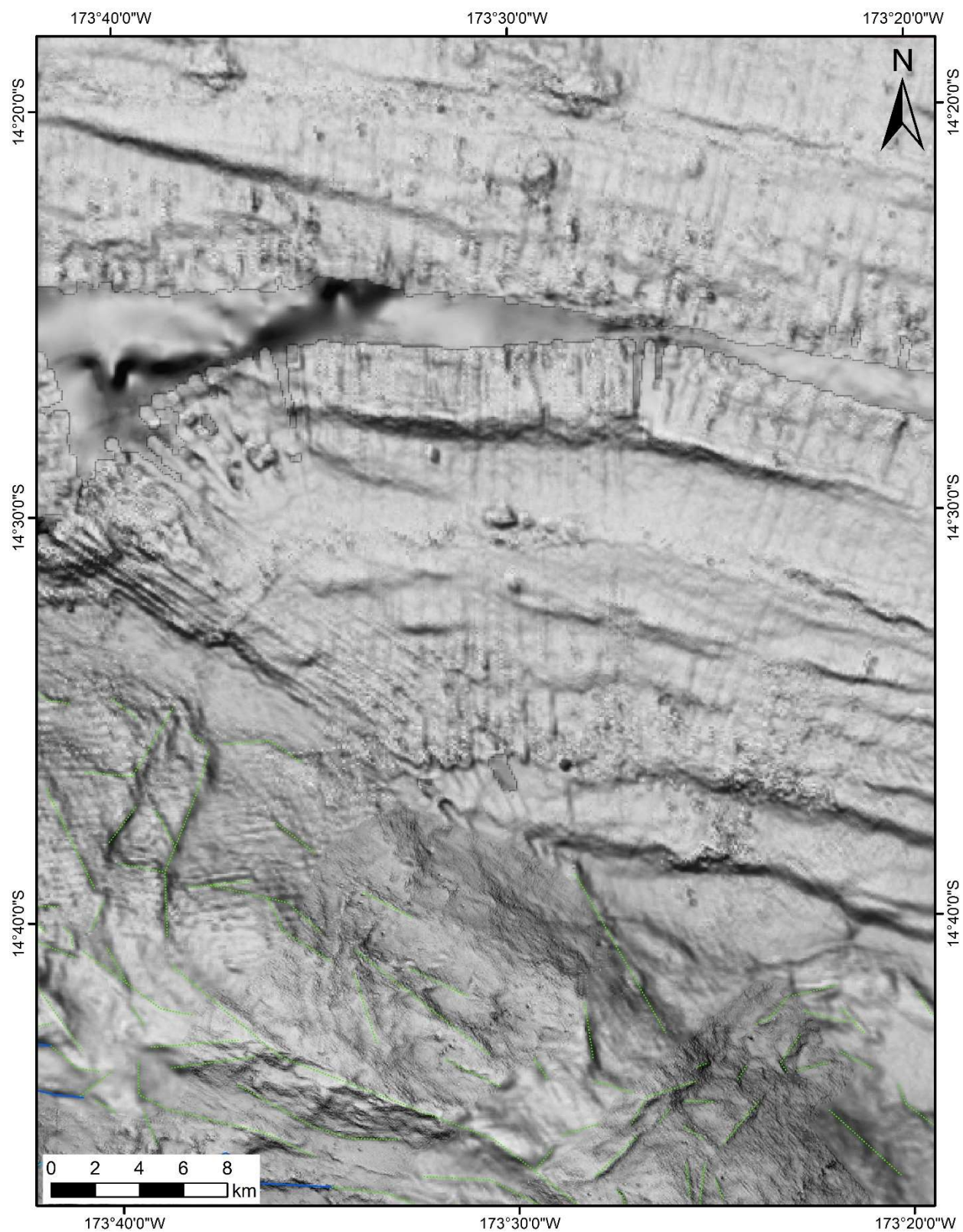


**Supplementary Figure S9.** Close-up of manually interpreted structures overlain on grayscale-shaded bathymetry, with the location shown on **Supplementary Fig. S6**. Major faults are dark blue, minor faults are light blue, volcanic ridges are red, and lineaments are green.

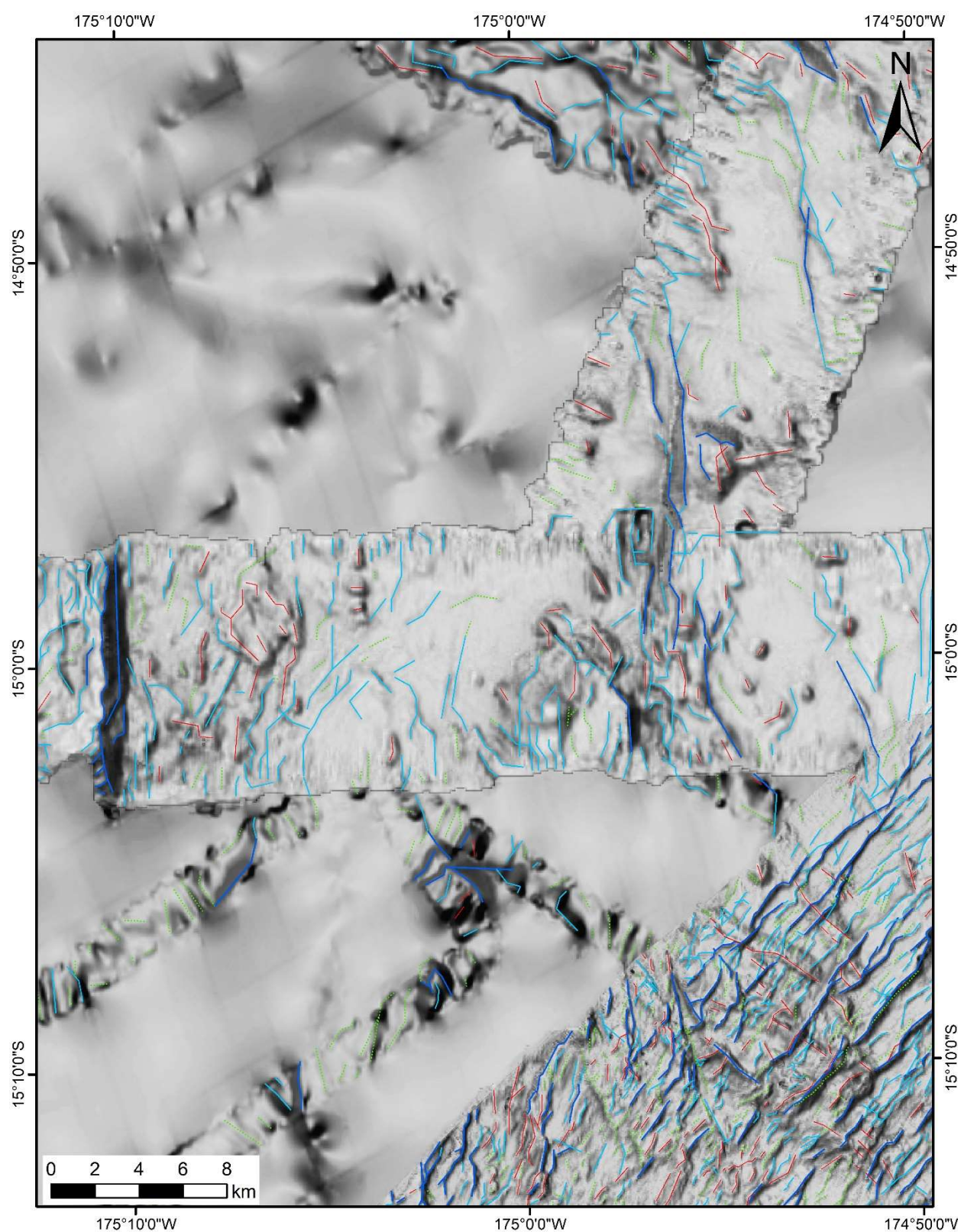




**Supplementary Figure S10.** Close-up of manually interpreted structures overlain on grayscale-shaded bathymetry, with the location shown on **Supplementary Fig. S6**. Major faults are dark blue, minor faults are light blue, volcanic ridges are red, and lineaments are green.

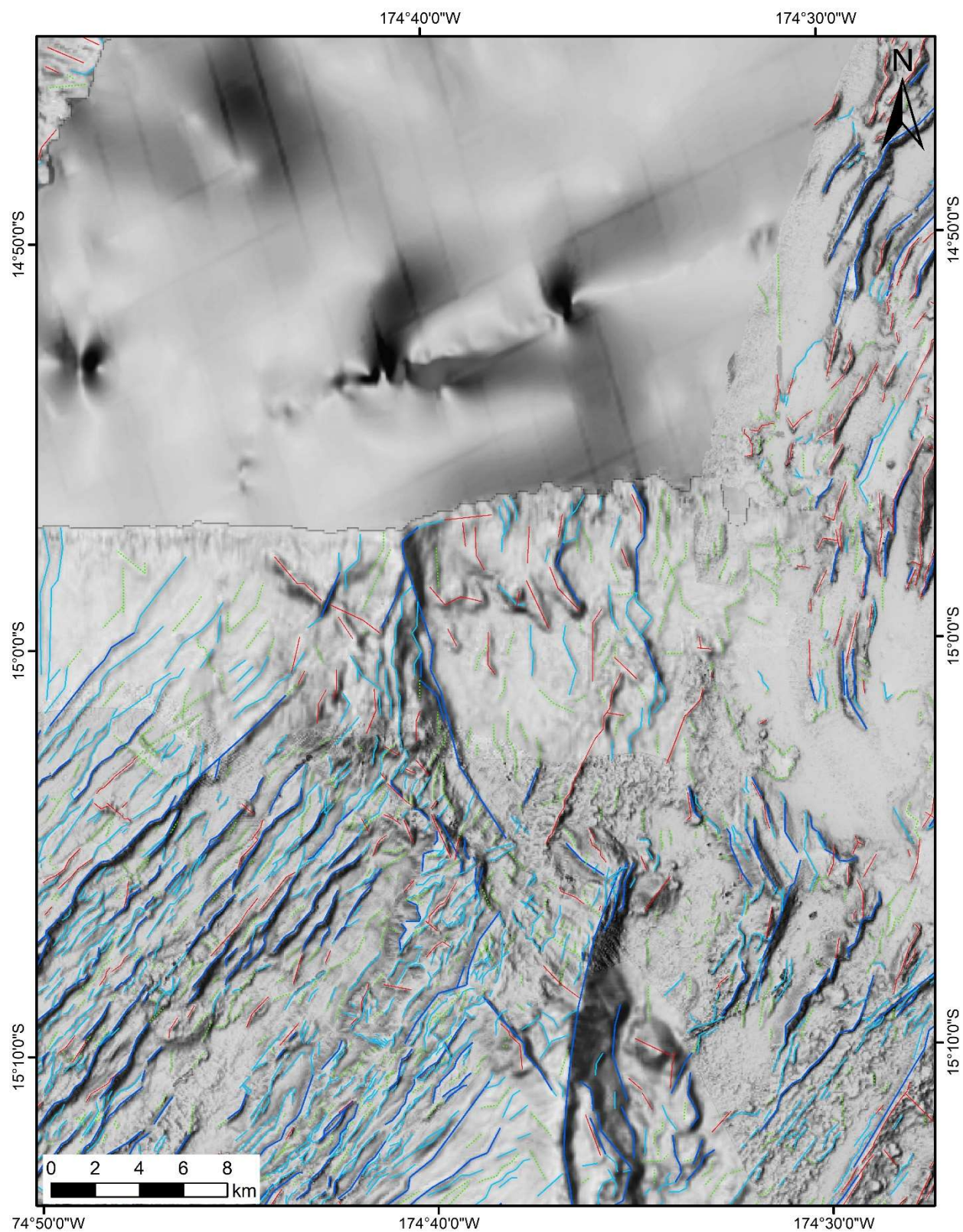


**Supplementary Figure S11.** Close-up of manually interpreted structures overlain on grayscale-shaded bathymetry, with the location shown on **Supplementary Fig. S6**. Major faults are dark blue, minor faults are light blue, volcanic ridges are red, and lineaments are green.



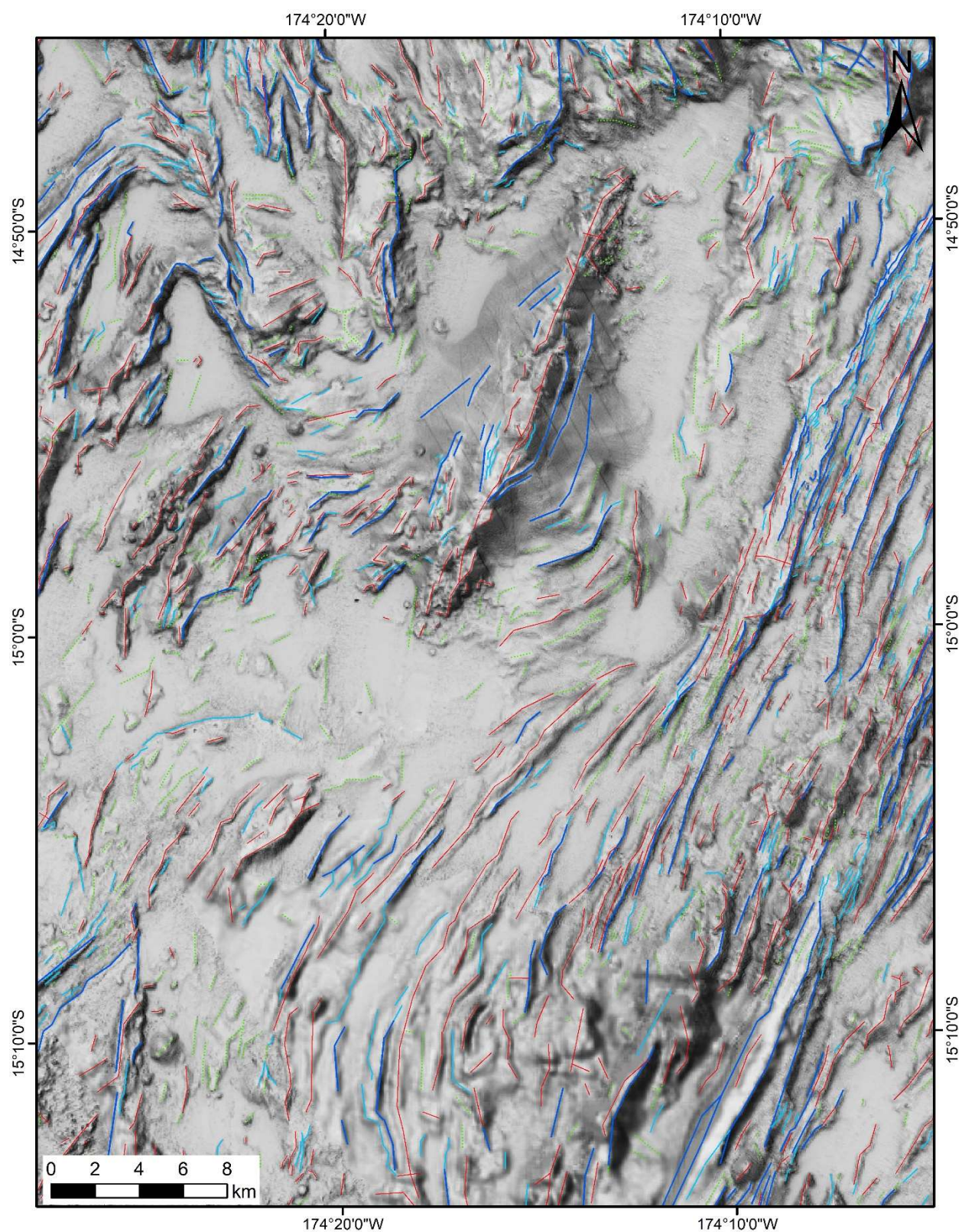


**Supplementary Figure S12.** Close-up of manually interpreted structures overlain on grayscale-shaded bathymetry, with the location shown on **Supplementary Fig. S6**. Major faults are dark blue, minor faults are light blue, volcanic ridges are red, and lineaments are green.



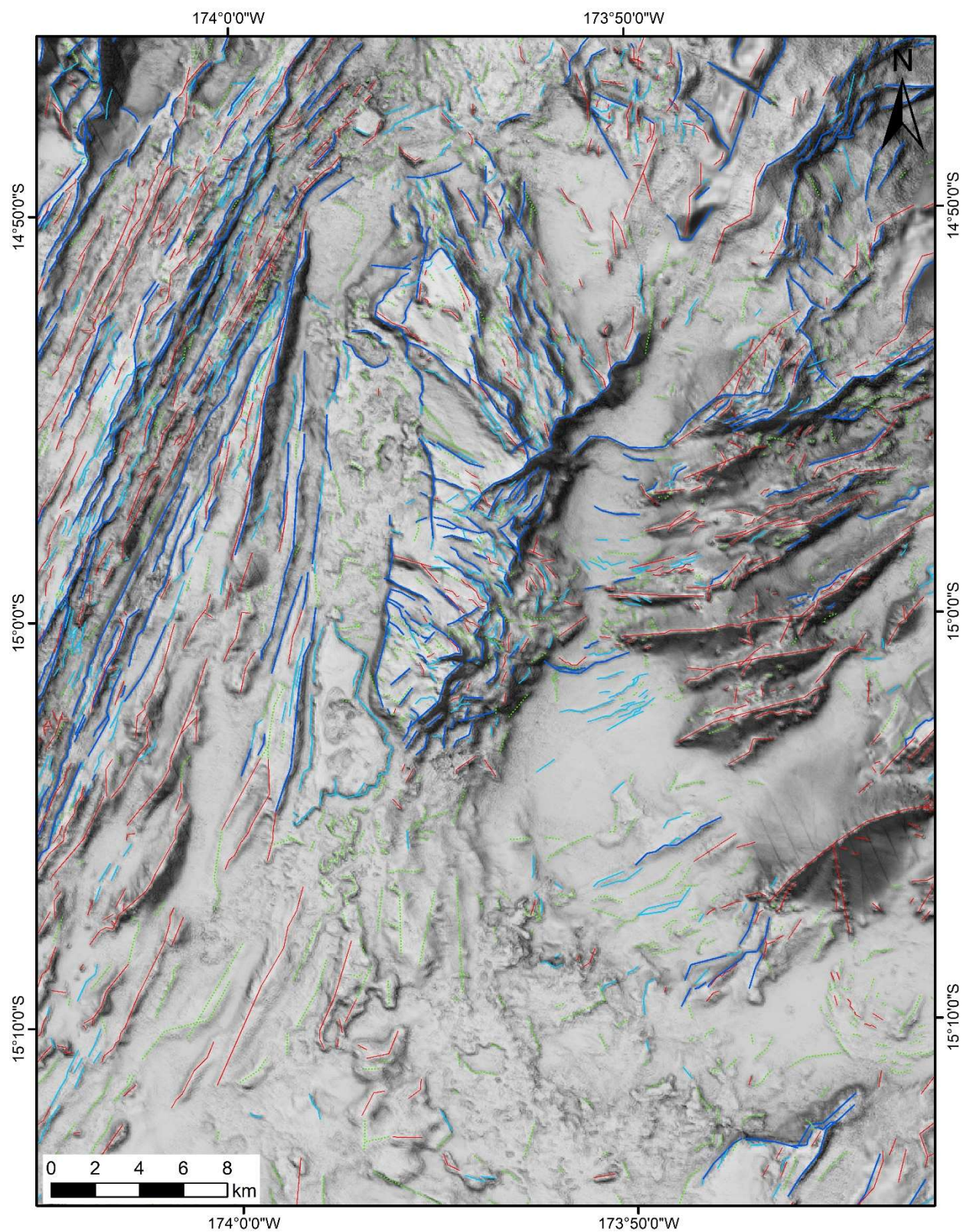


**Supplementary Figure S13.** Close-up of manually interpreted structures overlain on grayscale-shaded bathymetry, with the location shown on **Supplementary Fig. S6**. Major faults are dark blue, minor faults are light blue, volcanic ridges are red, and lineaments are green.



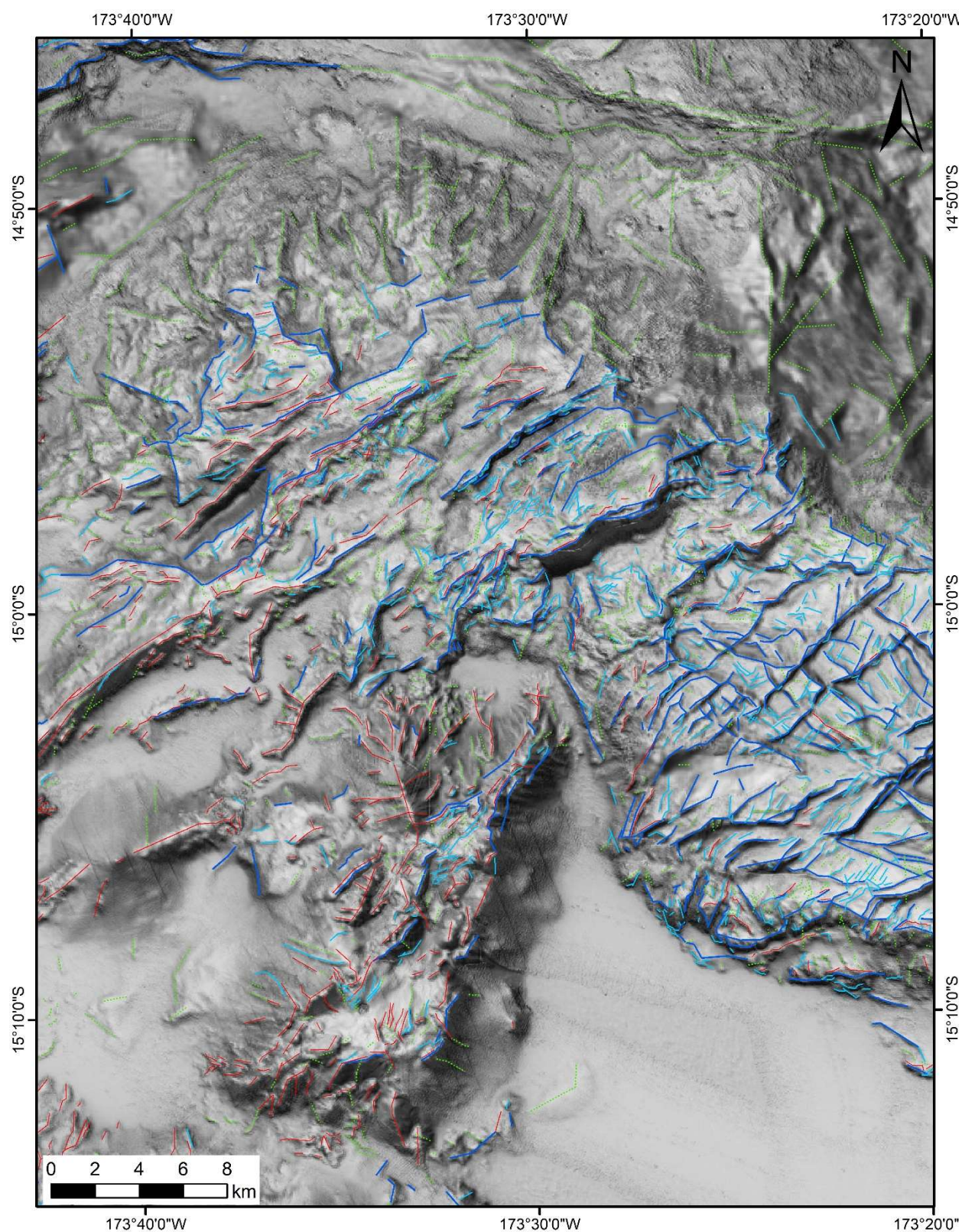


**Supplementary Figure S14.** Close-up of manually interpreted structures overlain on grayscale-shaded bathymetry, with the location shown on **Supplementary Fig. S6**. Major faults are dark blue, minor faults are light blue, volcanic ridges are red, and lineaments are green.



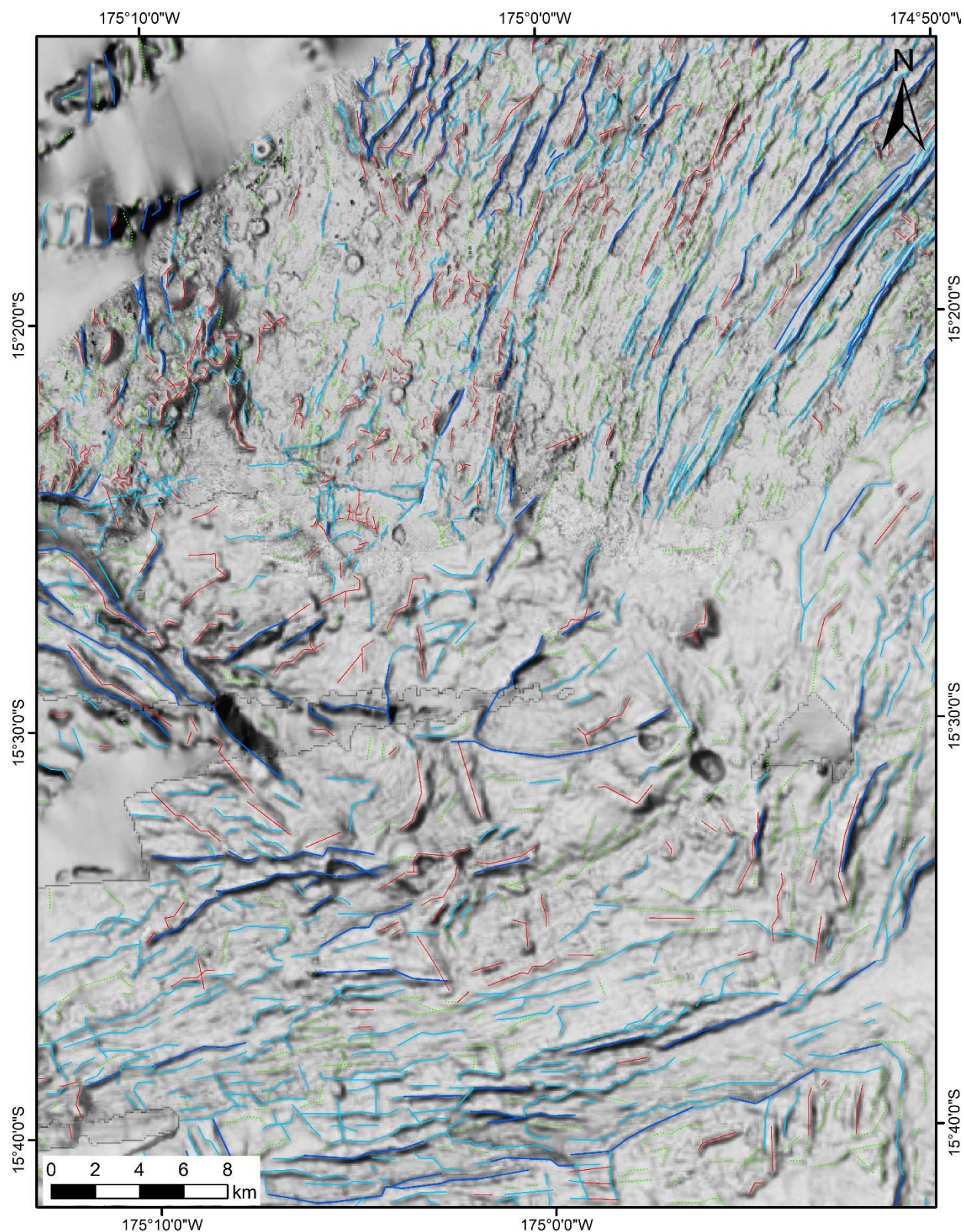


**Supplementary Figure S15.** Close-up of manually interpreted structures overlain on grayscale-shaded bathymetry, with the location shown on **Supplementary Fig. S6**. Major faults are dark blue, minor faults are light blue, volcanic ridges are red, and lineaments are green.



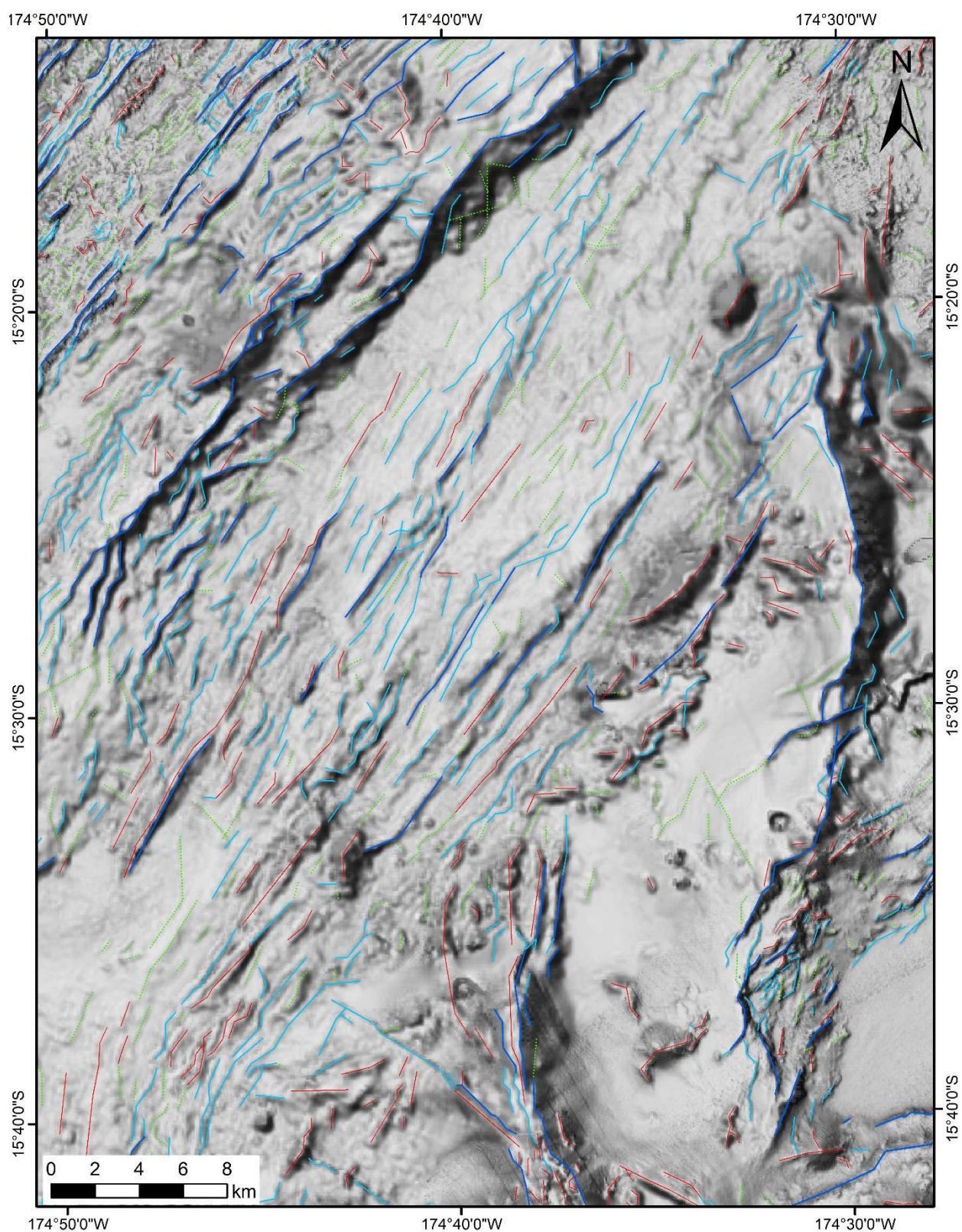


**Supplementary Figure S16.** Close-up of manually interpreted structures overlain on grayscale-shaded bathymetry, with the location shown on **Supplementary Fig. S6**. Major faults are dark blue, minor faults are light blue, volcanic ridges are red, and lineaments are green.



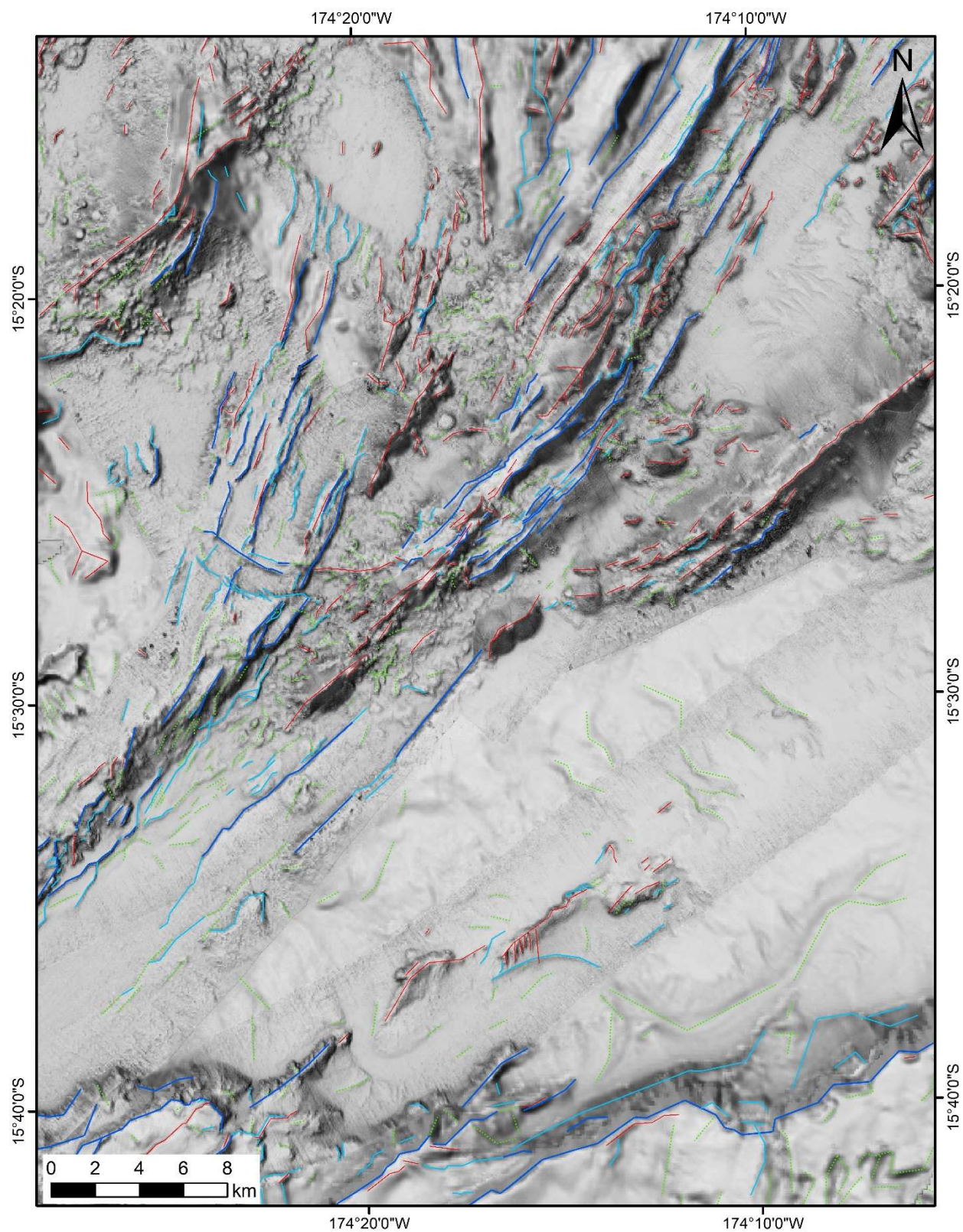


**Supplementary Figure S17.** Close-up of manually interpreted structures overlain on grayscale-shaded bathymetry, with the location shown on **Supplementary Fig. S6**. Major faults are dark blue, minor faults are light blue, volcanic ridges are red, and lineaments are green.



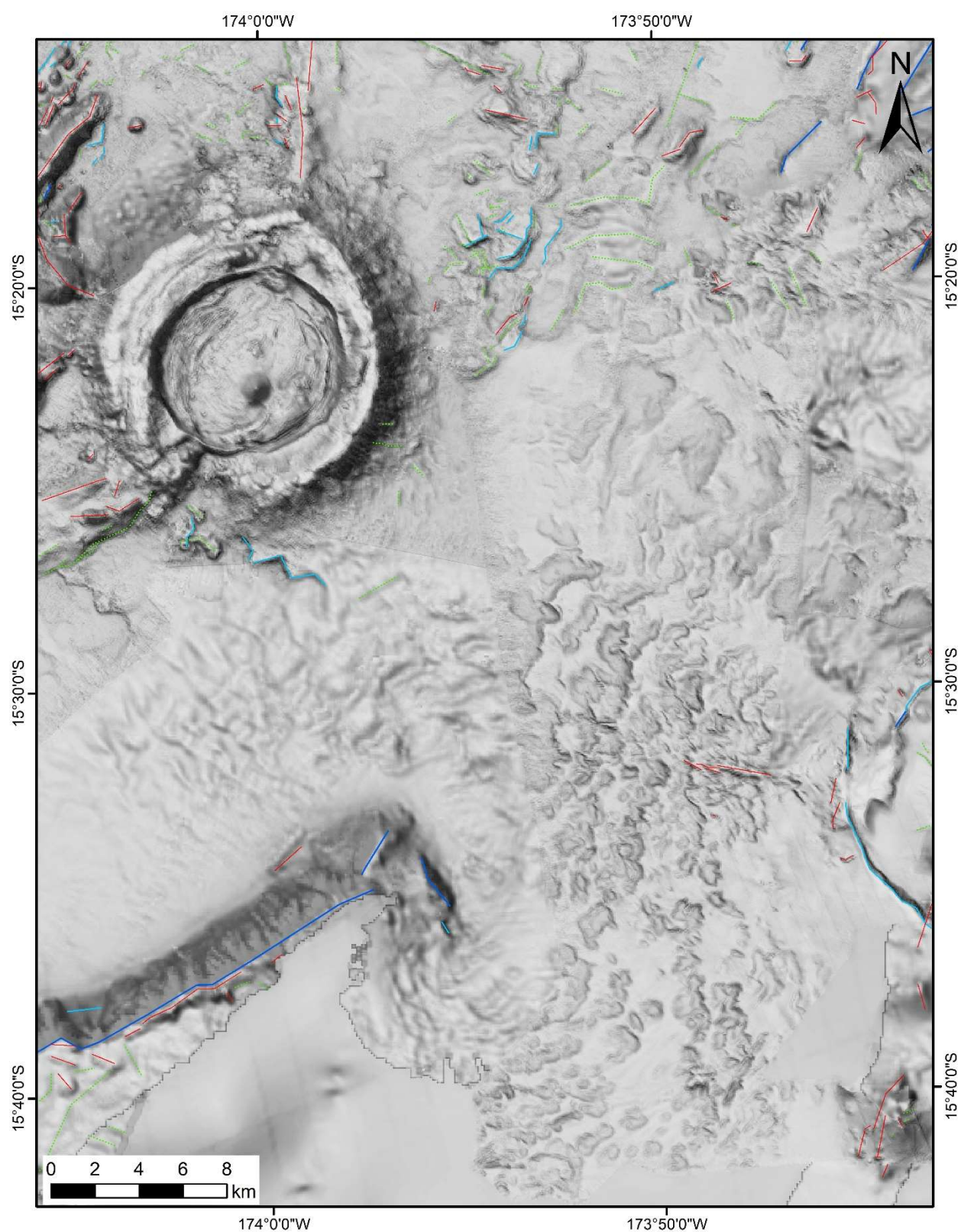


**Supplementary Figure S18.** Close-up of manually interpreted structures overlain on grayscale-shaded bathymetry, with the location shown on **Supplementary Fig. S6**. Major faults are dark blue, minor faults are light blue, volcanic ridges are red, and lineaments are green.



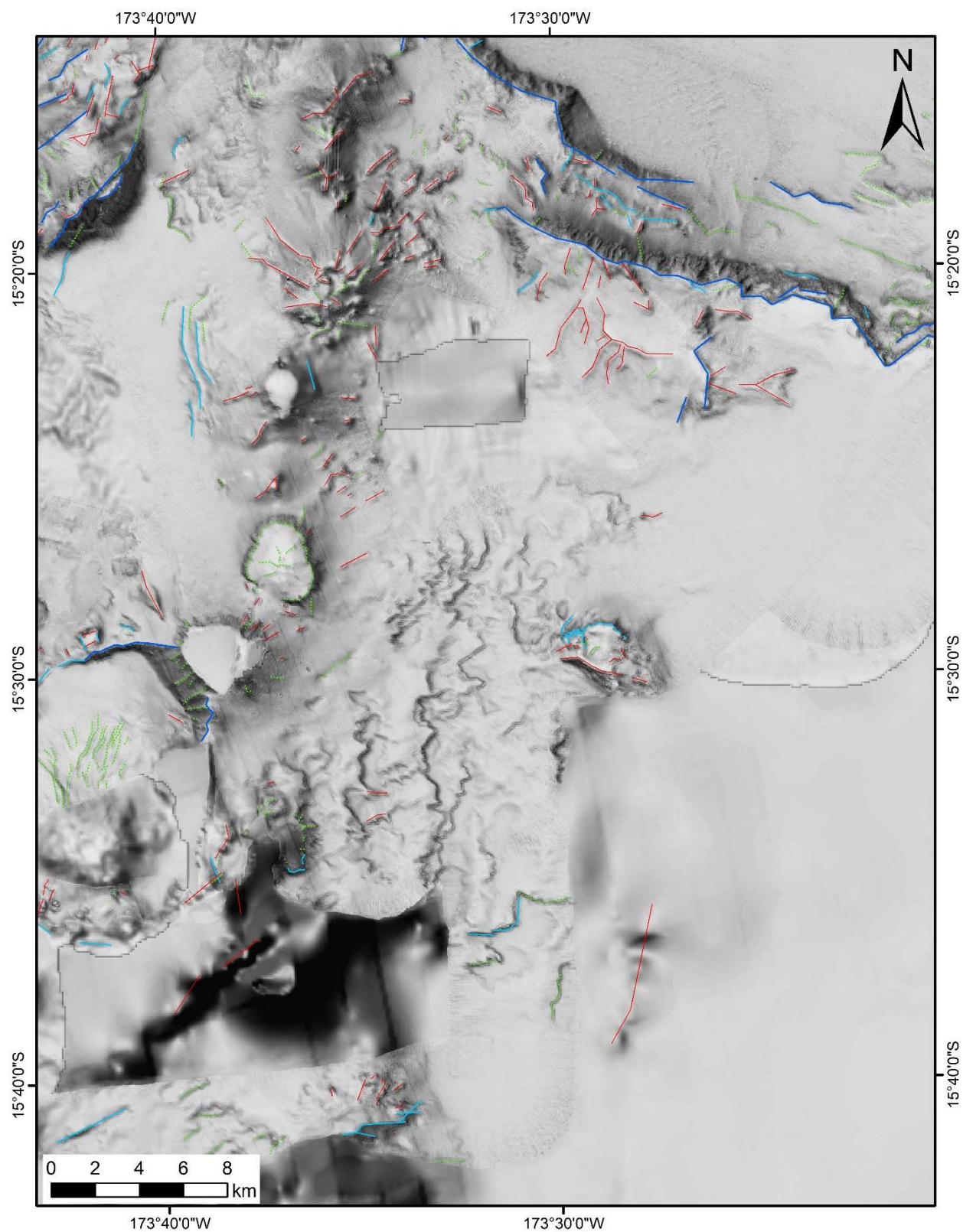


**Supplementary Figure S19.** Close-up of manually interpreted structures overlain on grayscale-shaded bathymetry, with the location shown on **Supplementary Fig. S6**. Major faults are dark blue, minor faults are light blue, volcanic ridges are red, and lineaments are green.



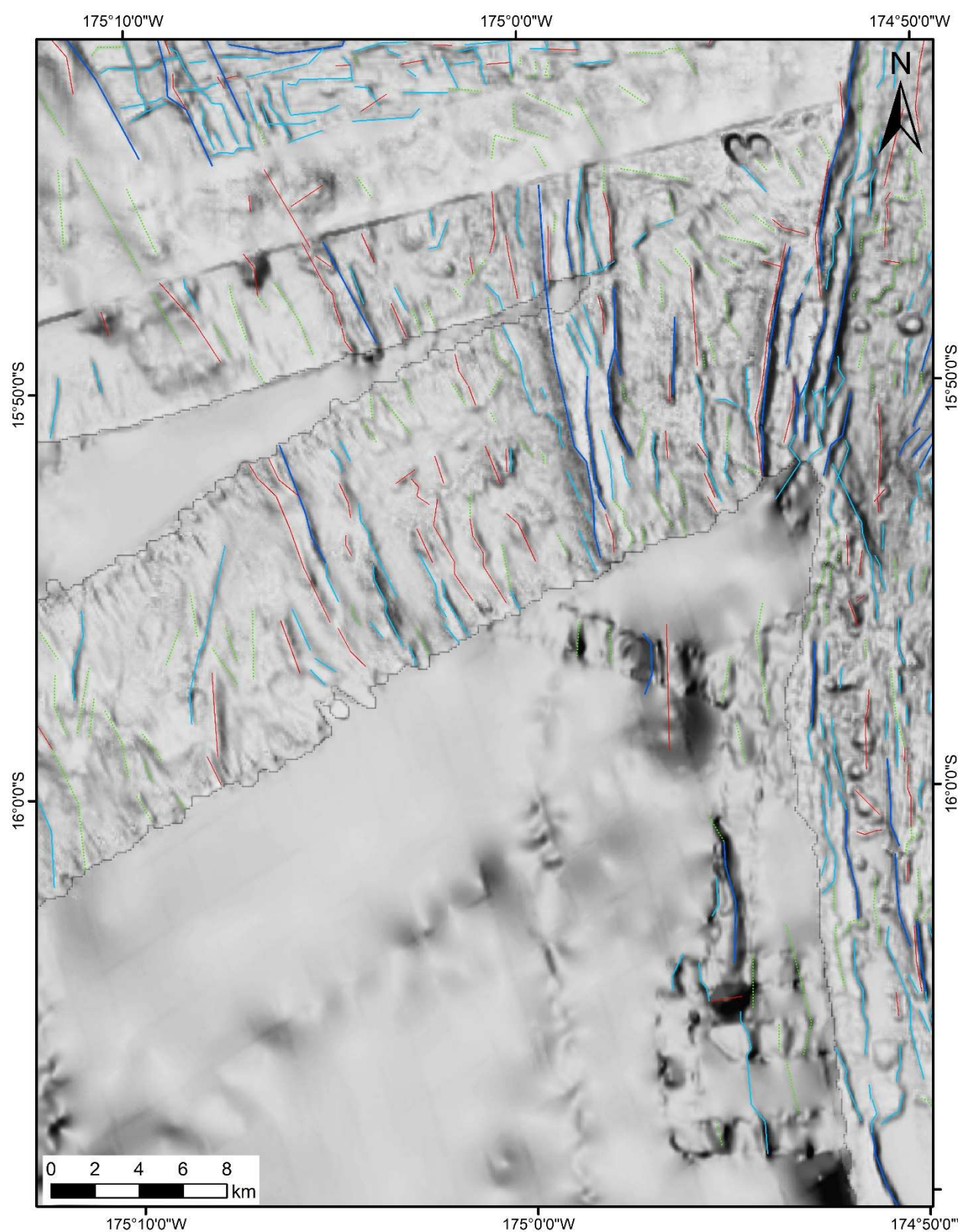


**Supplementary Figure S20.** Close-up of manually interpreted structures overlain on grayscale-shaded bathymetry, with the location shown on **Supplementary Fig. S6**. Major faults are dark blue, minor faults are light blue, volcanic ridges are red, and lineaments are green.



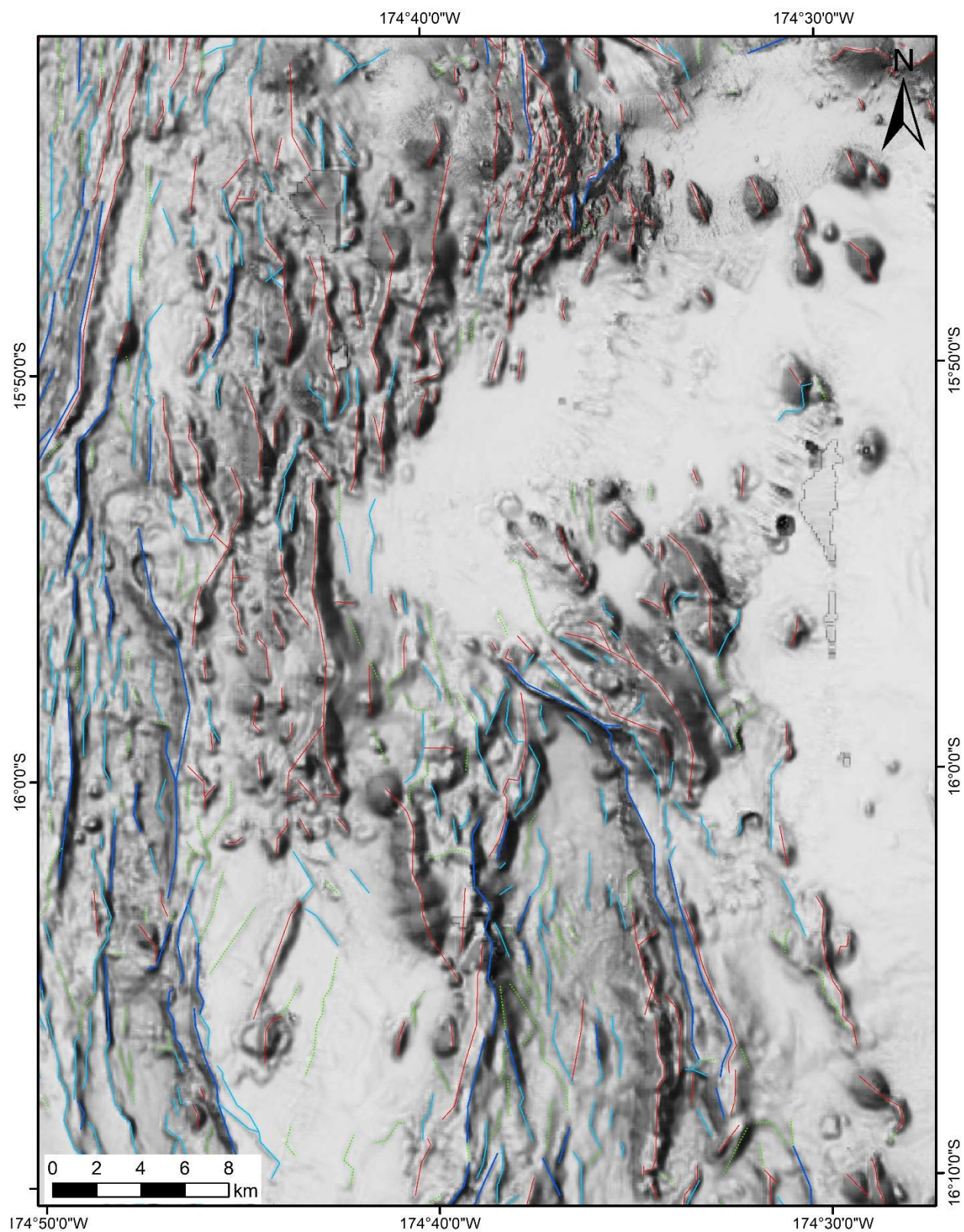


**Supplementary Figure S21.** Close-up of manually interpreted structures overlain on grayscale-shaded bathymetry, with the location shown on **Supplementary Fig. S6**. Major faults are dark blue, minor faults are light blue, volcanic ridges are red, and lineaments are green.



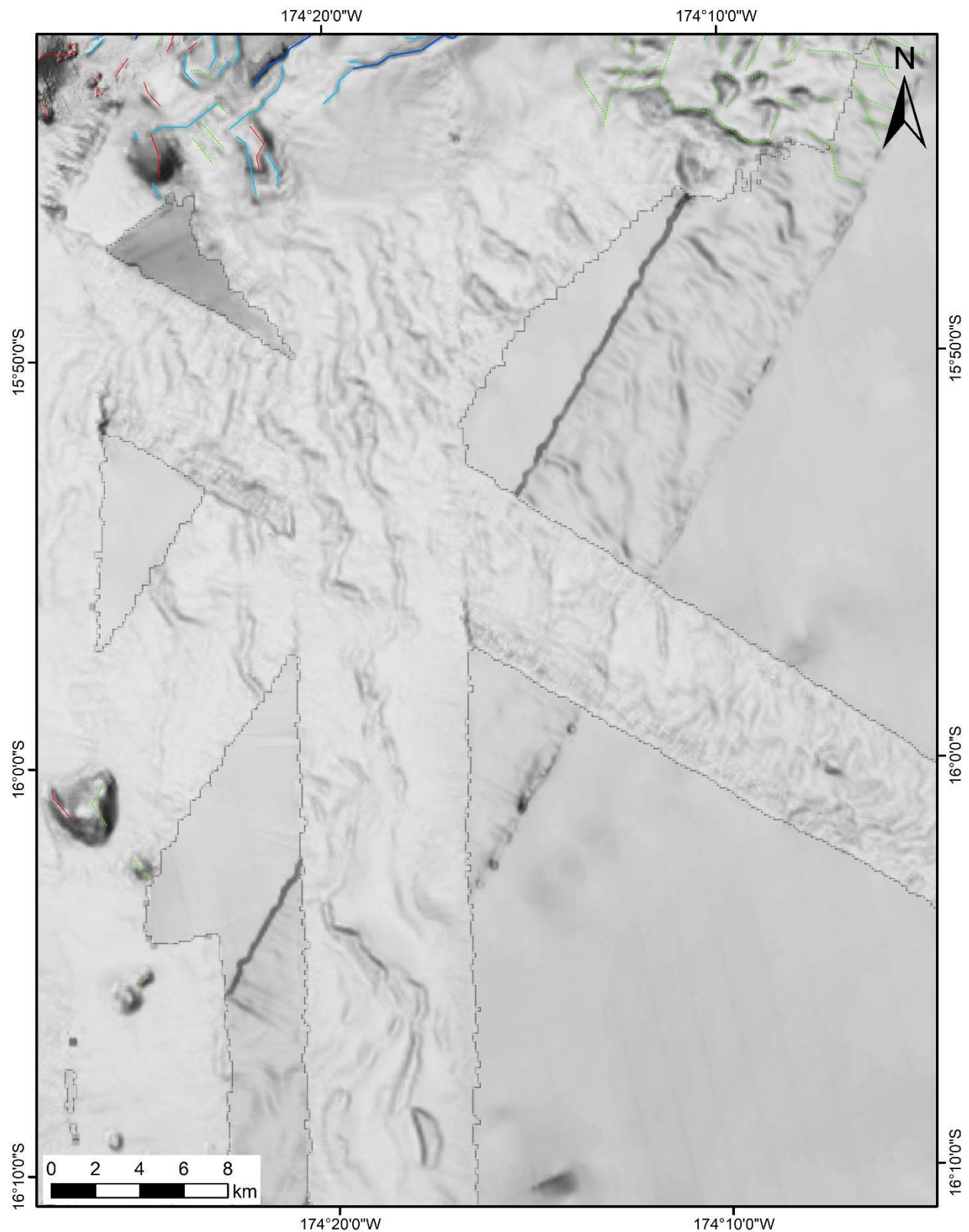


**Supplementary Figure S22.** Close-up of manually interpreted structures overlain on grayscale-shaded bathymetry, with the location shown on **Supplementary Fig. S6**. Major faults are dark blue, minor faults are light blue, volcanic ridges are red, and lineaments are green.



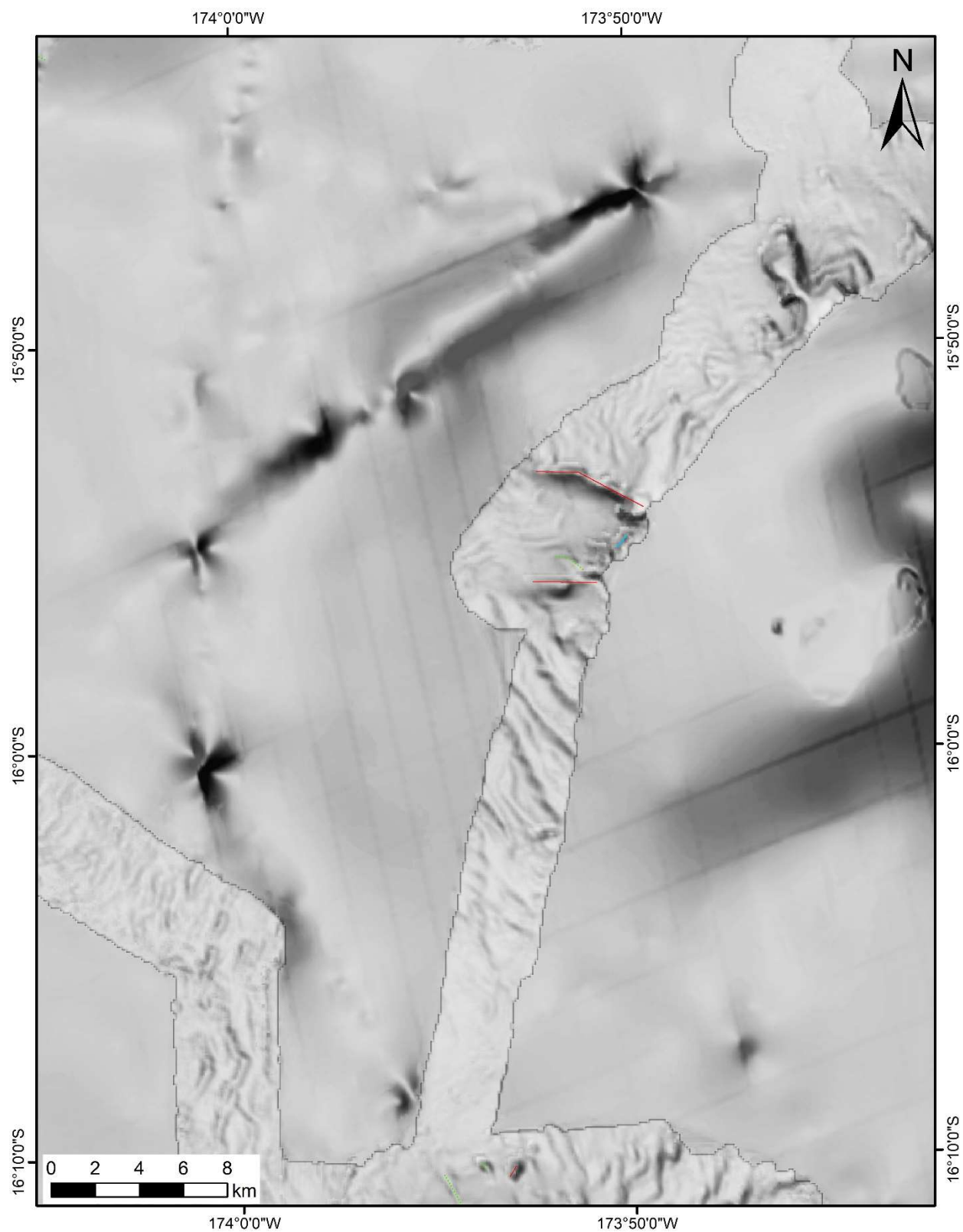


**Supplementary Figure S23.** Close-up of manually interpreted structures overlain on grayscale-shaded bathymetry, with the location shown on **Supplementary Fig. S6**. Major faults are dark blue, minor faults are light blue, volcanic ridges are red, and lineaments are green.



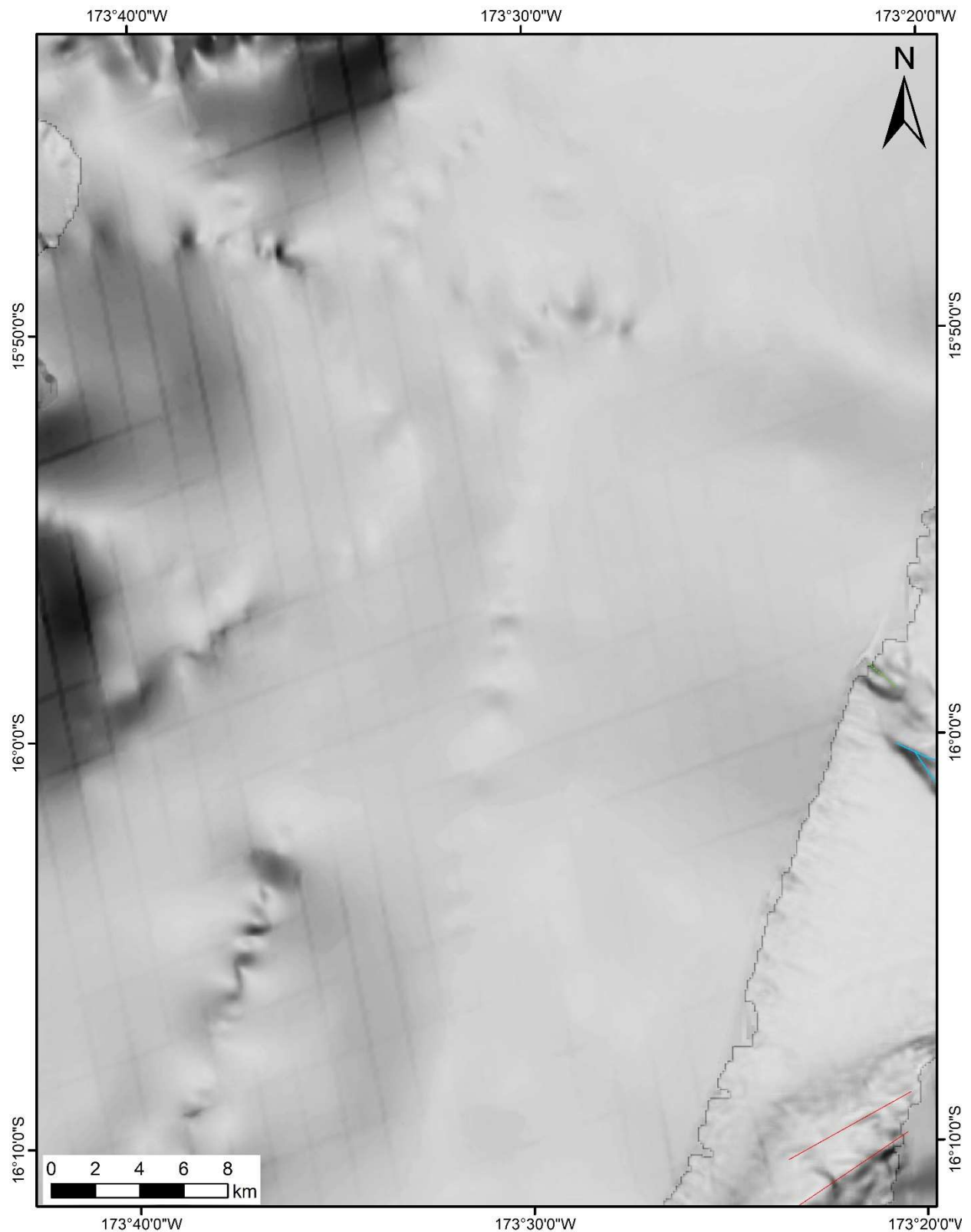


**Supplementary Figure S24.** Close-up of manually interpreted structures overlain on grayscale-shaded bathymetry, with the location shown on **Supplementary Fig. S6**. Major faults are dark blue, minor faults are light blue, volcanic ridges are red, and lineaments are green.



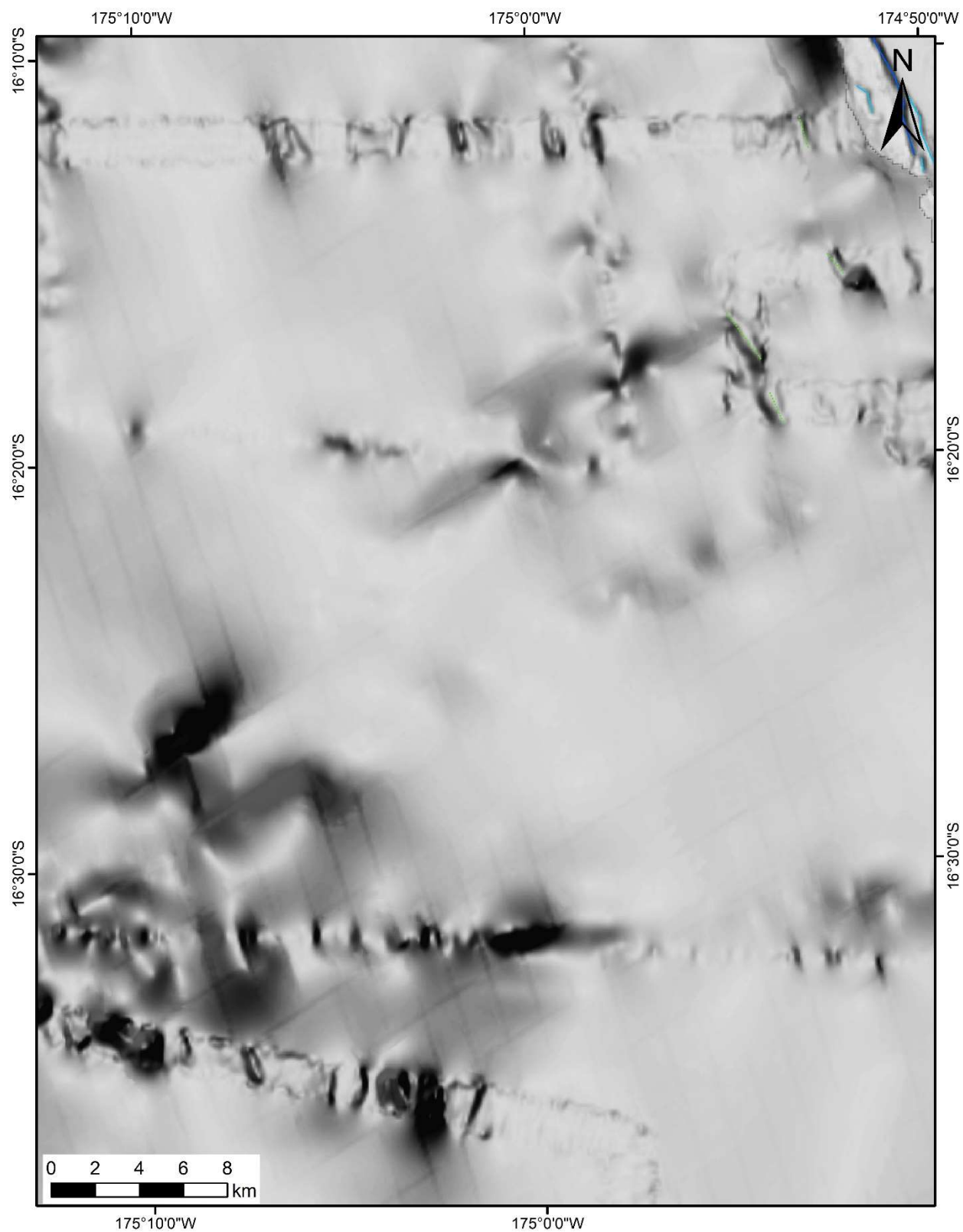


**Supplementary Figure S25.** Close-up of manually interpreted structures overlain on grayscale-shaded bathymetry, with the location shown on **Supplementary Fig. S6**. Major faults are dark blue, minor faults are light blue, volcanic ridges are red, and lineaments are green.



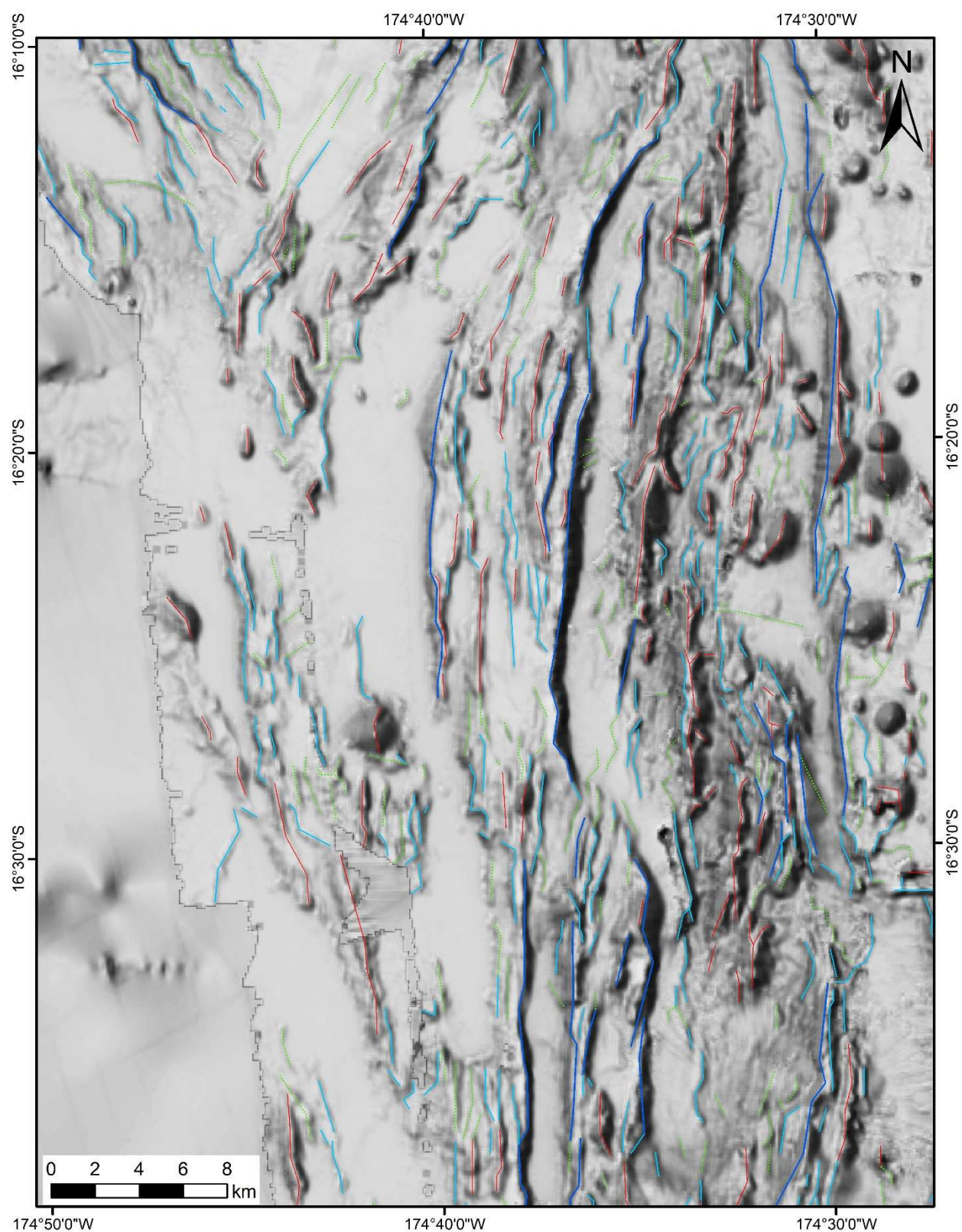


**Supplementary Figure S26.** Close-up of manually interpreted structures overlain on grayscale-shaded bathymetry, with the location shown on **Supplementary Fig. S6**. Major faults are dark blue, minor faults are light blue, volcanic ridges are red, and lineaments are green.



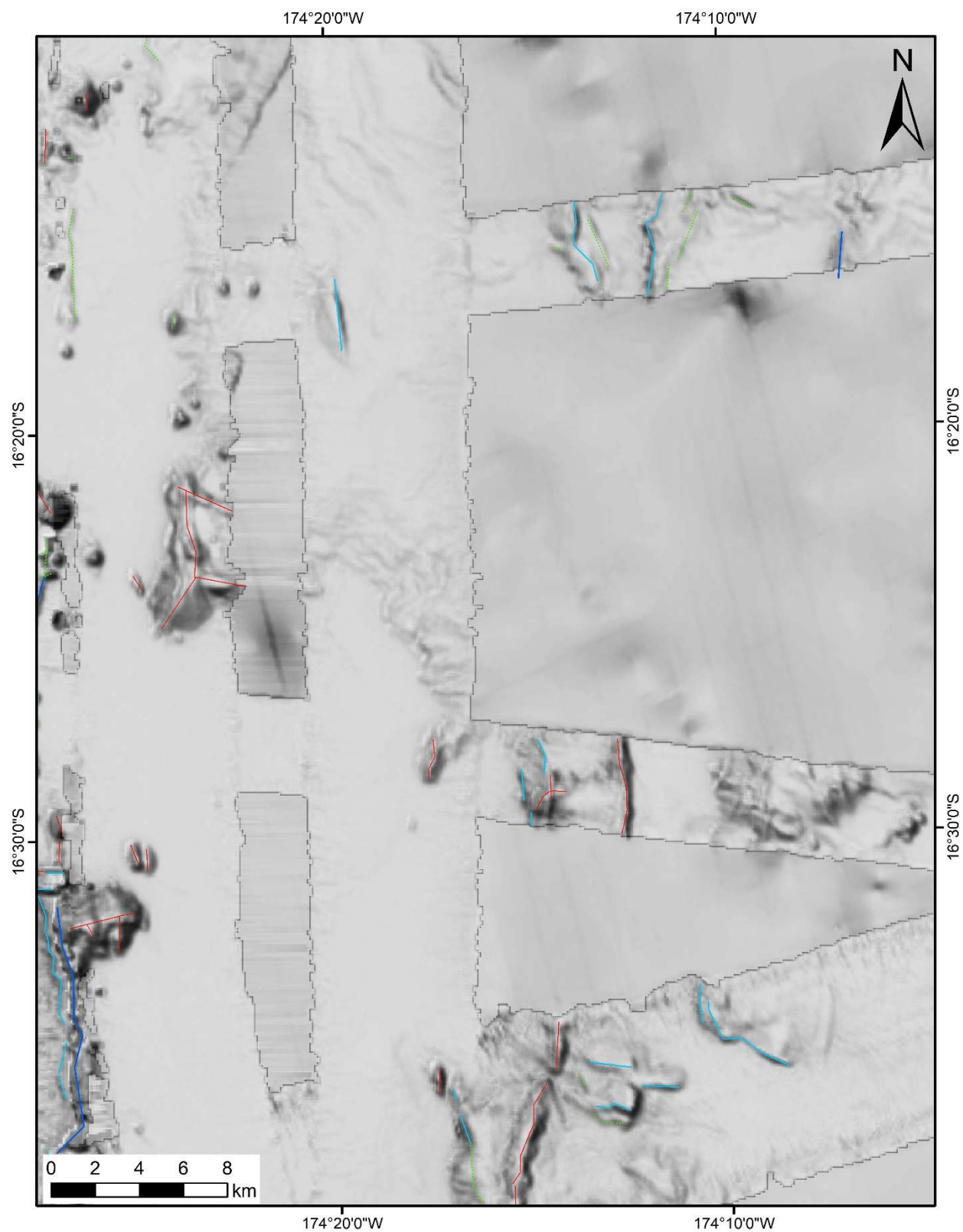


**Supplementary Figure S27.** Close-up of manually interpreted structures overlain on grayscale-shaded bathymetry, with the location shown on **Supplementary Fig. S6**. Major faults are dark blue, minor faults are light blue, volcanic ridges are red, and lineaments are green.

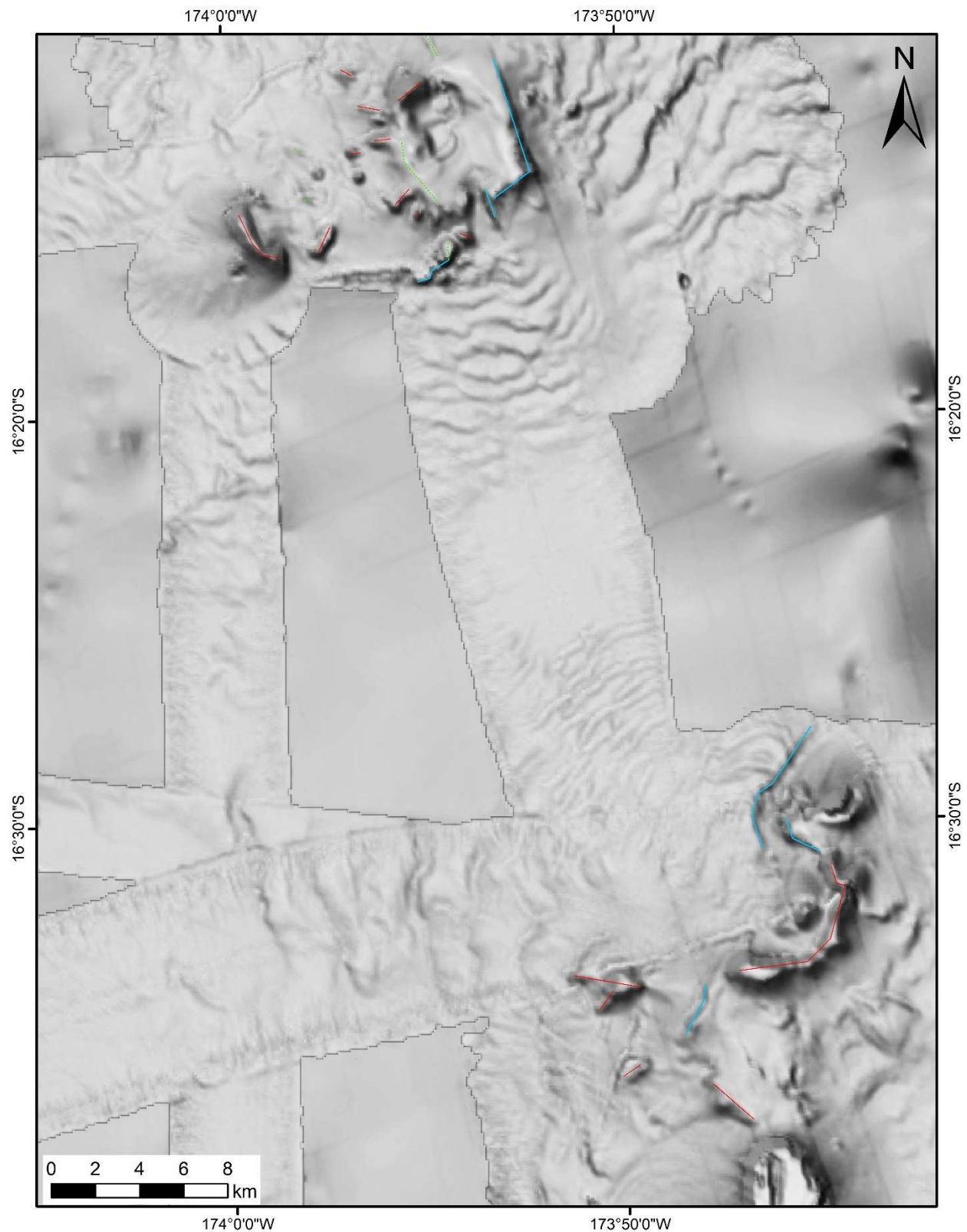




**Supplementary Figure S28.** Close-up of manually interpreted structures overlain on grayscale-shaded bathymetry, with the location shown on **Supplementary Fig. S6**. Major faults are dark blue, minor faults are light blue, volcanic ridges are red, and lineaments are green.

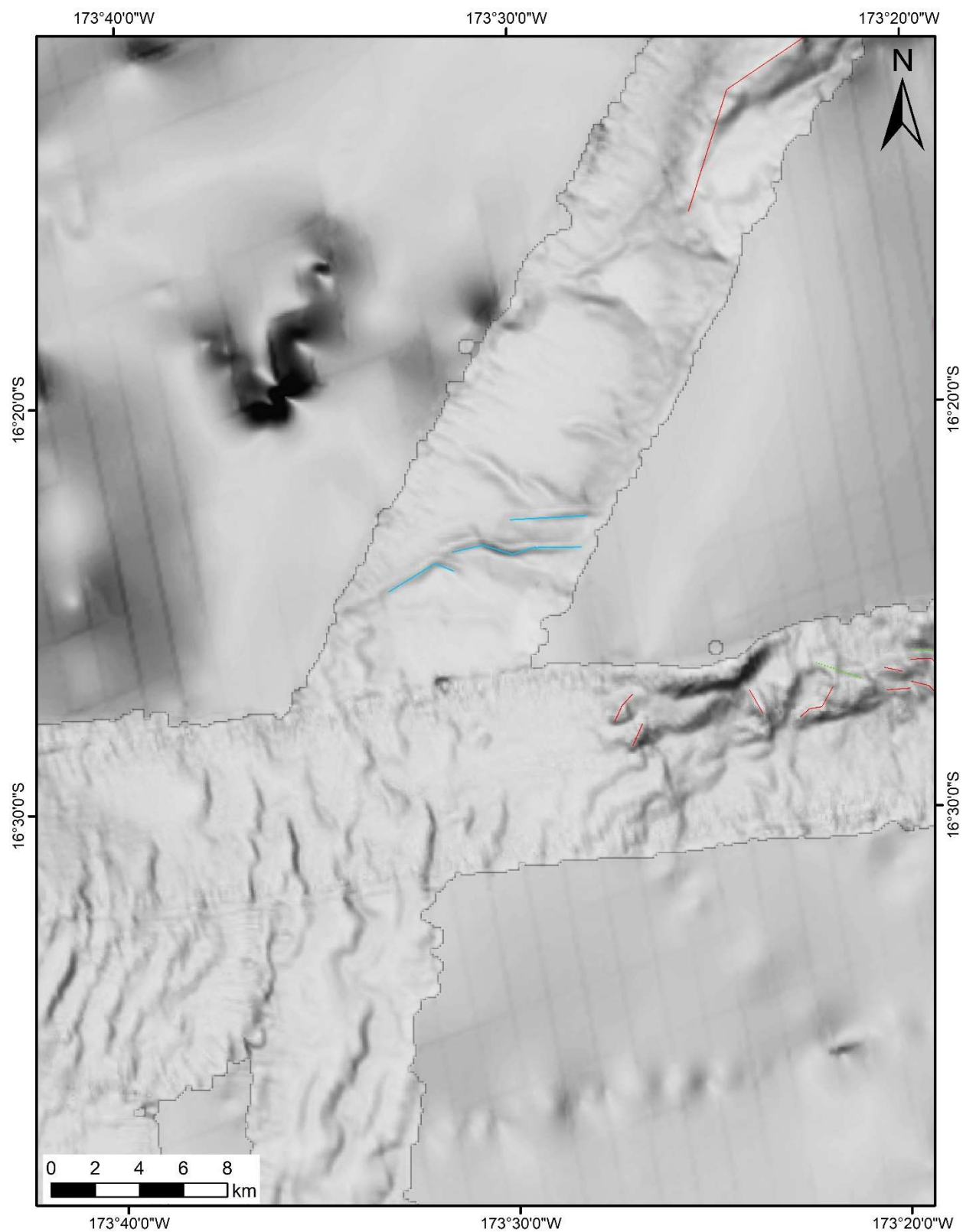


**Supplementary Figure S29.** Close-up of manually interpreted structures overlain on grayscale-shaded bathymetry, with the location shown on **Supplementary Fig. S6**. Major faults are dark blue, minor faults are light blue, volcanic ridges are red, and lineaments are green.

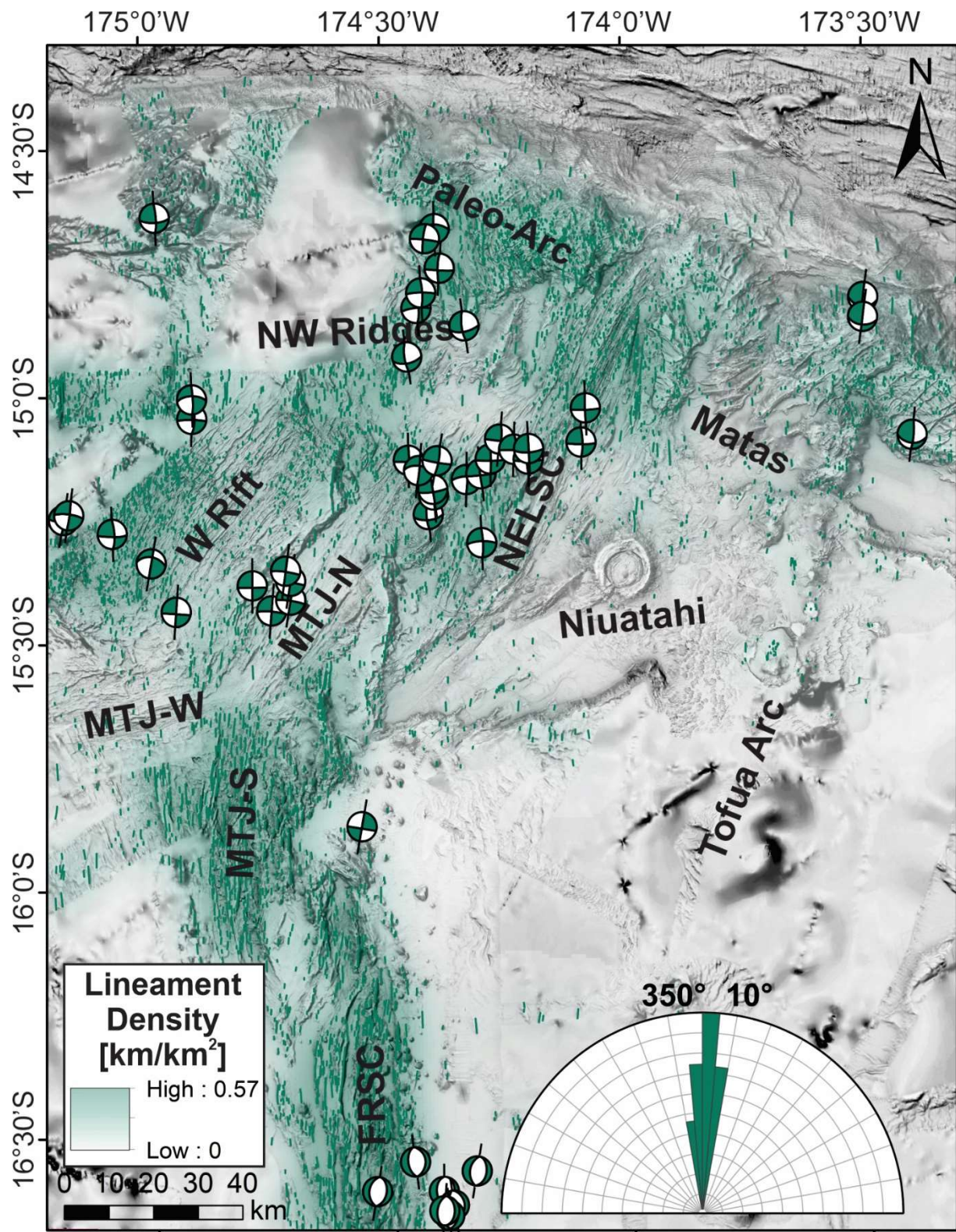




**Supplementary Figure S30.** Close-up of manually interpreted structures overlain on grayscale-shaded bathymetry, with the location shown on **Supplementary Fig. S6**. Major faults are dark blue, minor faults are light blue, volcanic ridges are red, and lineaments are green.

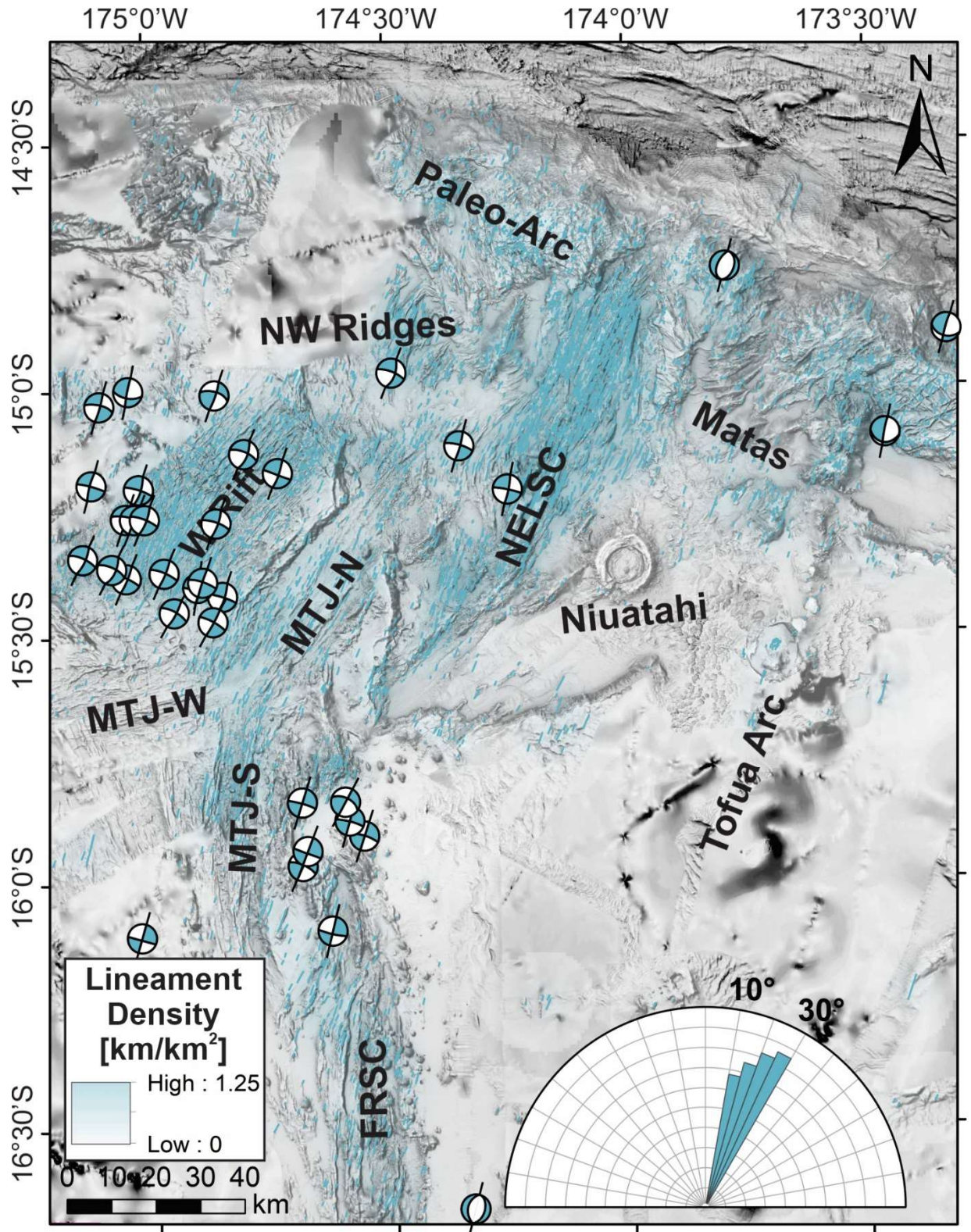


**Supplementary Figure S31.** Close-up of manually interpreted structures overlain on grayscale-shaded bathymetry, with the location shown on **Supplementary Fig. S6**. Major faults are dark blue, minor faults are light blue, volcanic ridges are red, and lineaments are green.



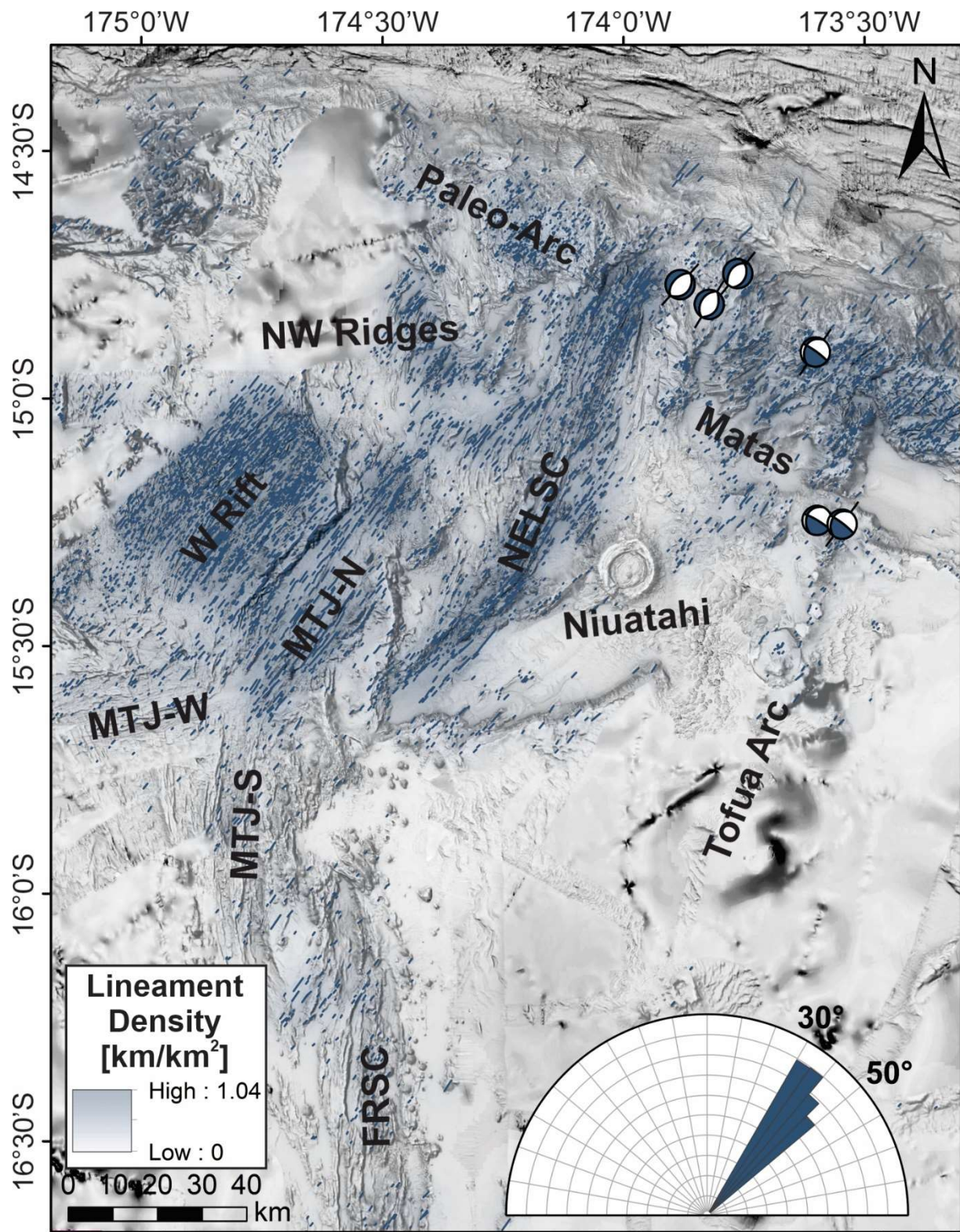


**Supplementary Figure S32.** Close-up of interpreted N-trending structural lineaments (**Fig. 7a**), relative lineament densities ( $\text{km per km}^2$ ) and shallow ( $\leq 25 \text{ km}$ ) CMT focal plane solutions ([www.globalcmt.org](http://www.globalcmt.org); Dziewonski et al., 1981; Ekström et al., 2012). Abbreviations as in **Figure 2**.



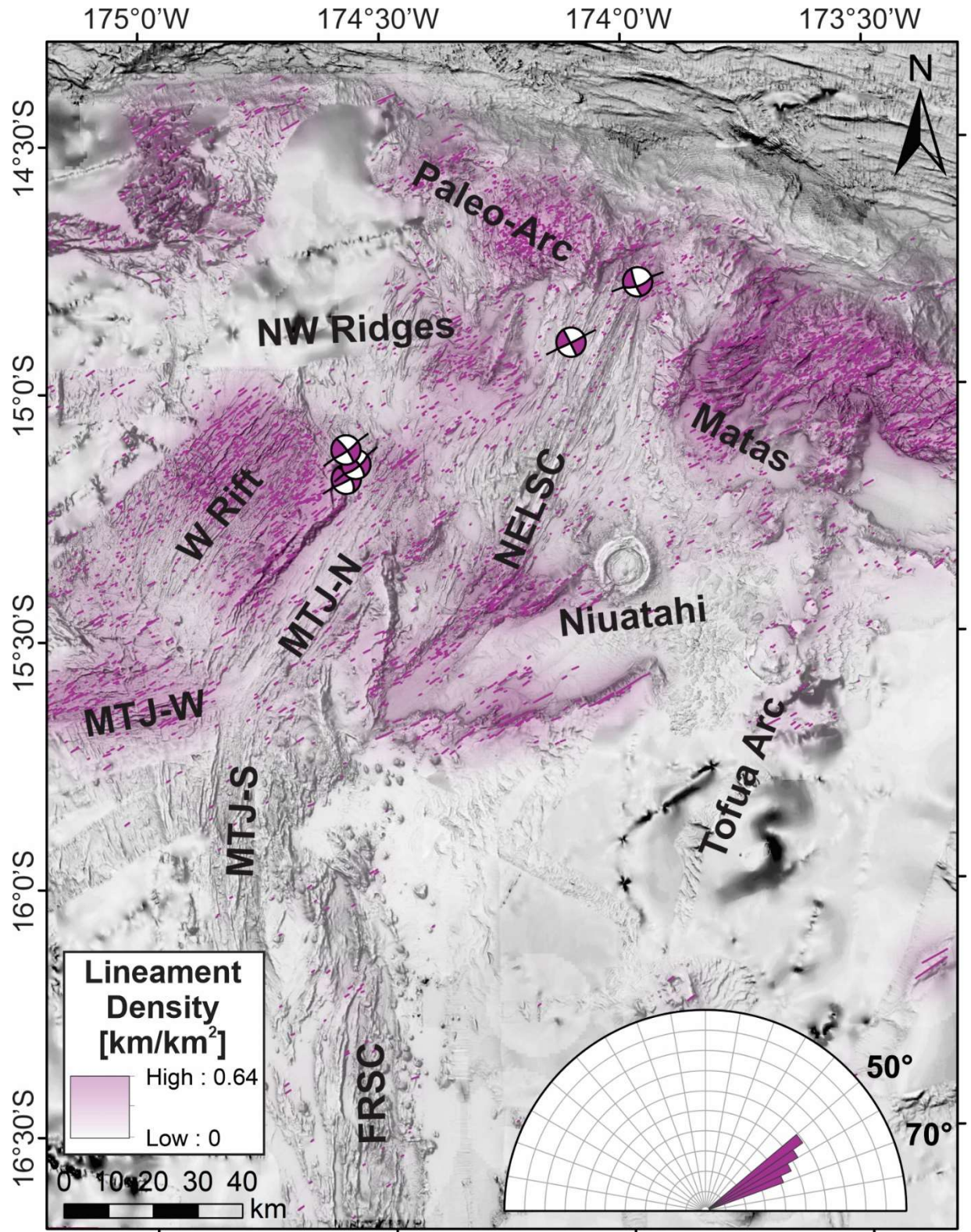


**Supplementary Figure S33.** Close-up of interpreted NNE-trending structural lineaments (**Fig. 7b**), relative lineament densities ( $\text{km per km}^2$ ) and shallow ( $\leq 25 \text{ km}$ ) CMT focal plane solutions ([www.globalcmt.org](http://www.globalcmt.org); Dziewonski et al., 1981; Ekström et al., 2012). Abbreviations as in **Figure 2**.



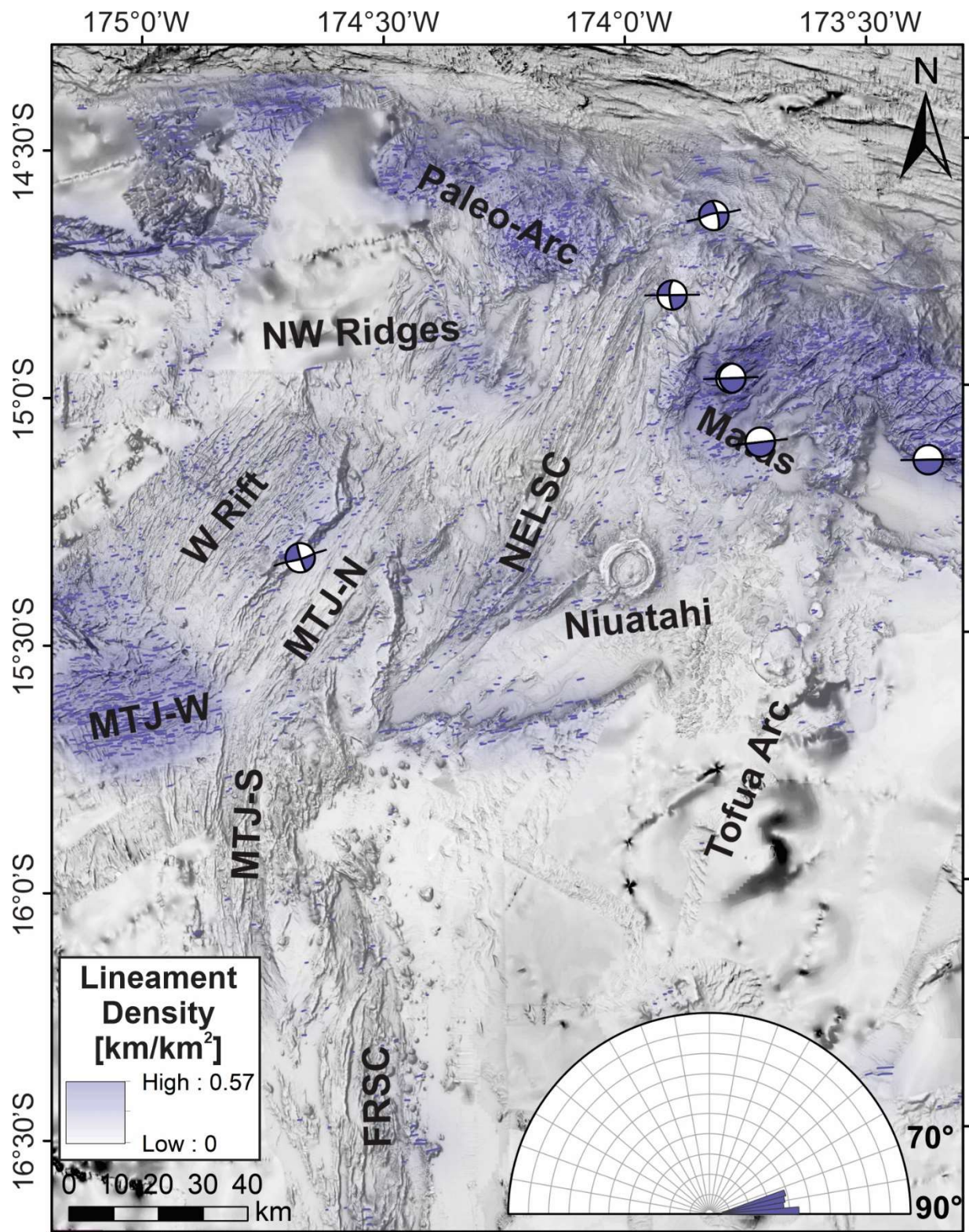


**Supplementary Figure S34.** Close-up of interpreted NE-trending structural lineaments (**Fig. 7c**), relative lineament densities ( $\text{km per km}^2$ ) and shallow ( $\leq 25 \text{ km}$ ) CMT focal plane solutions ([www.globalcmt.org](http://www.globalcmt.org); Dziewonski et al., 1981; Ekström et al., 2012). Abbreviations as in **Figure 2**.



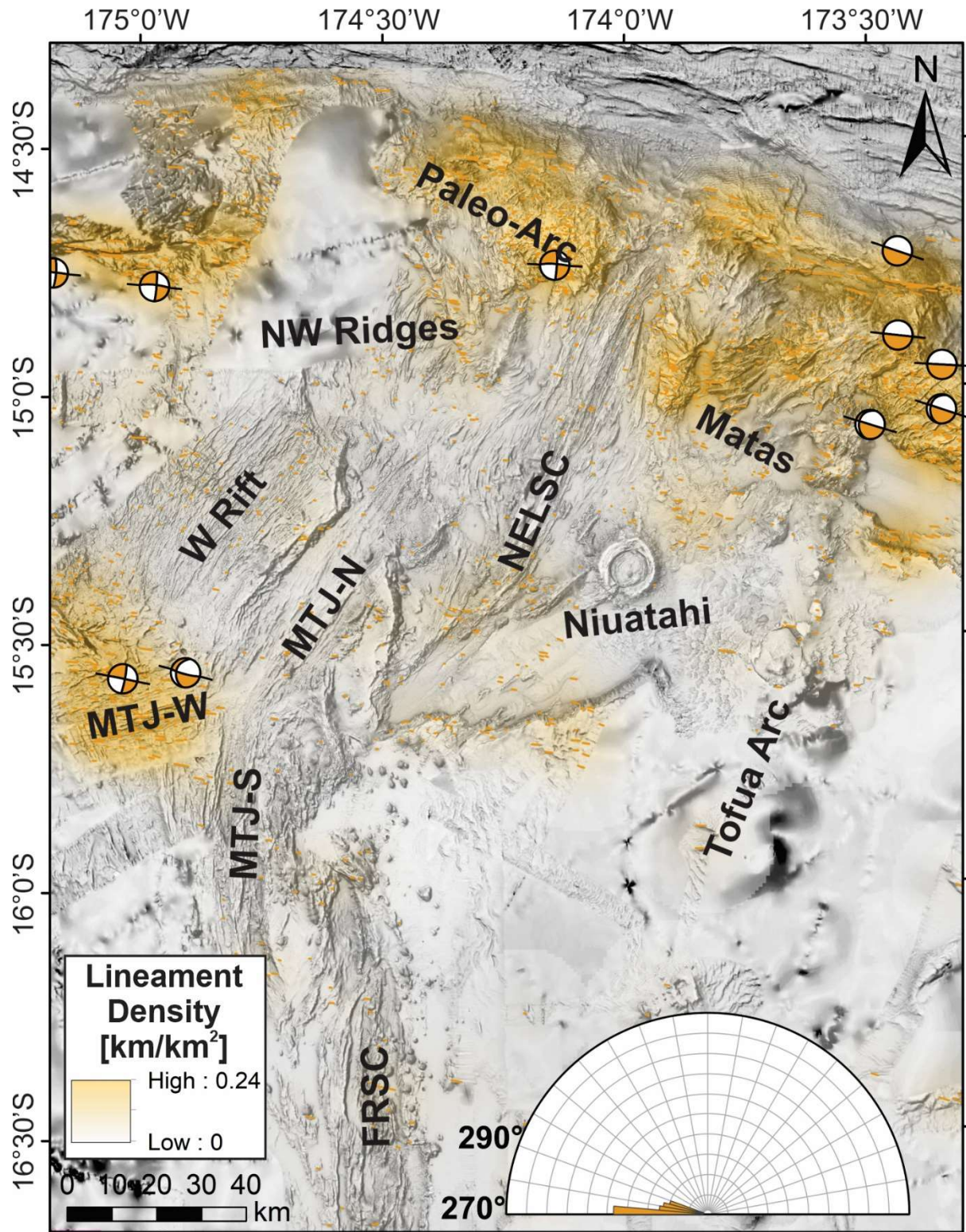


**Supplementary Figure S35.** Close-up of interpreted ENE-trending structural lineaments (**Fig. 7d**), relative lineament densities ( $\text{km per km}^2$ ) and shallow ( $\leq 25 \text{ km}$ ) CMT focal plane solutions ([www.globalcmt.org](http://www.globalcmt.org); Dziewonski et al., 1981; Ekström et al., 2012). Abbreviations as in **Figure 2**.



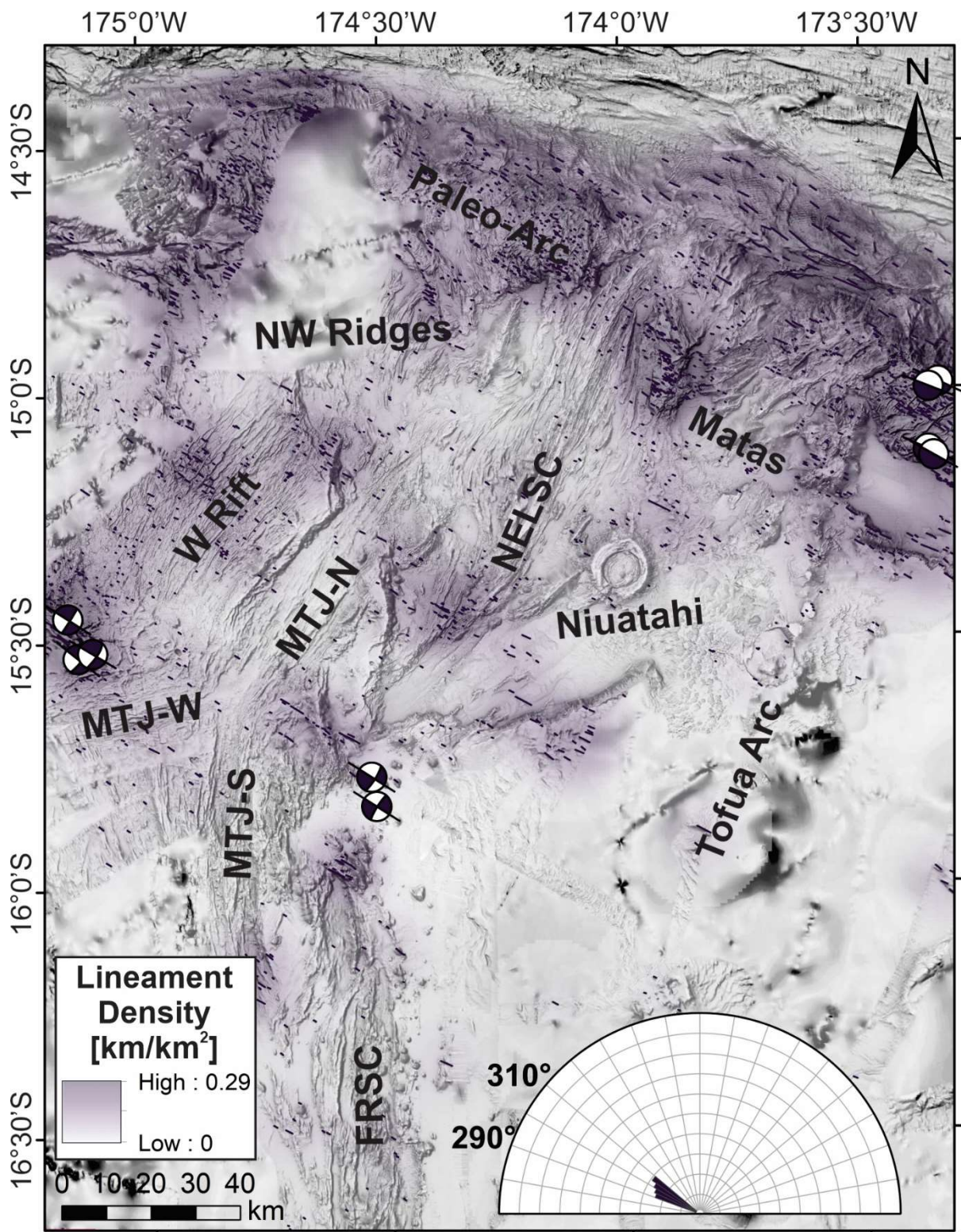


**Supplementary Figure S36.** Close-up of interpreted E-trending structural lineaments (**Fig. 7e**), relative lineament densities (km per km<sup>2</sup>) and shallow ( $\leq 25$  km) CMT focal plane solutions ([www.globalcmt.org](http://www.globalcmt.org); Dziewonski et al., 1981; Ekström et al., 2012). Abbreviations as in **Figure 2**.



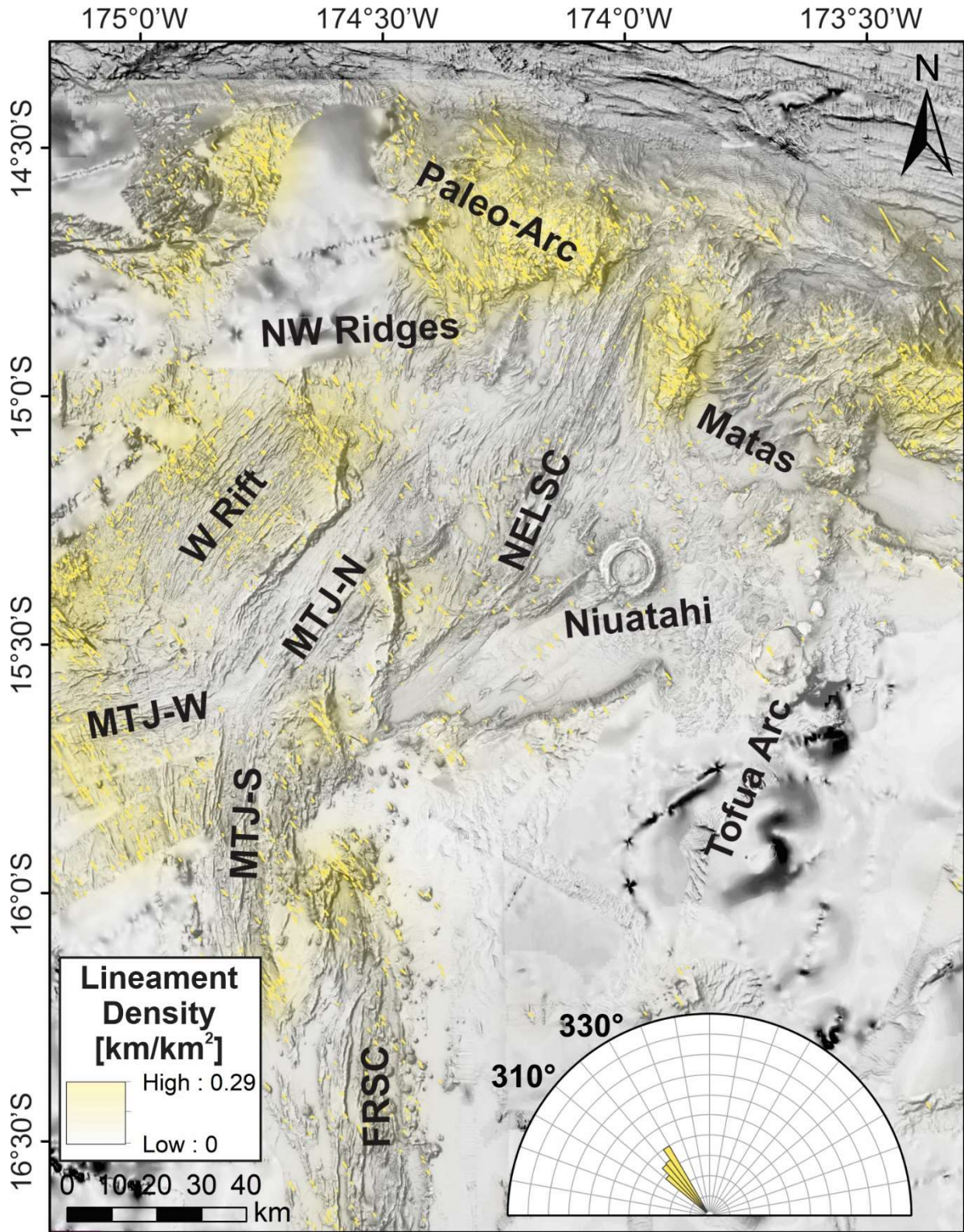


**Supplementary Figure S37.** Close-up of interpreted W-trending structural lineaments (**Fig. 7f**), relative lineament densities (km per km<sup>2</sup>) and shallow ( $\leq 25$  km) CMT focal plane solutions (www.globalcmt.org; Dziewonski et al., 1981; Ekström et al., 2012). Abbreviations as in **Figure 2**.



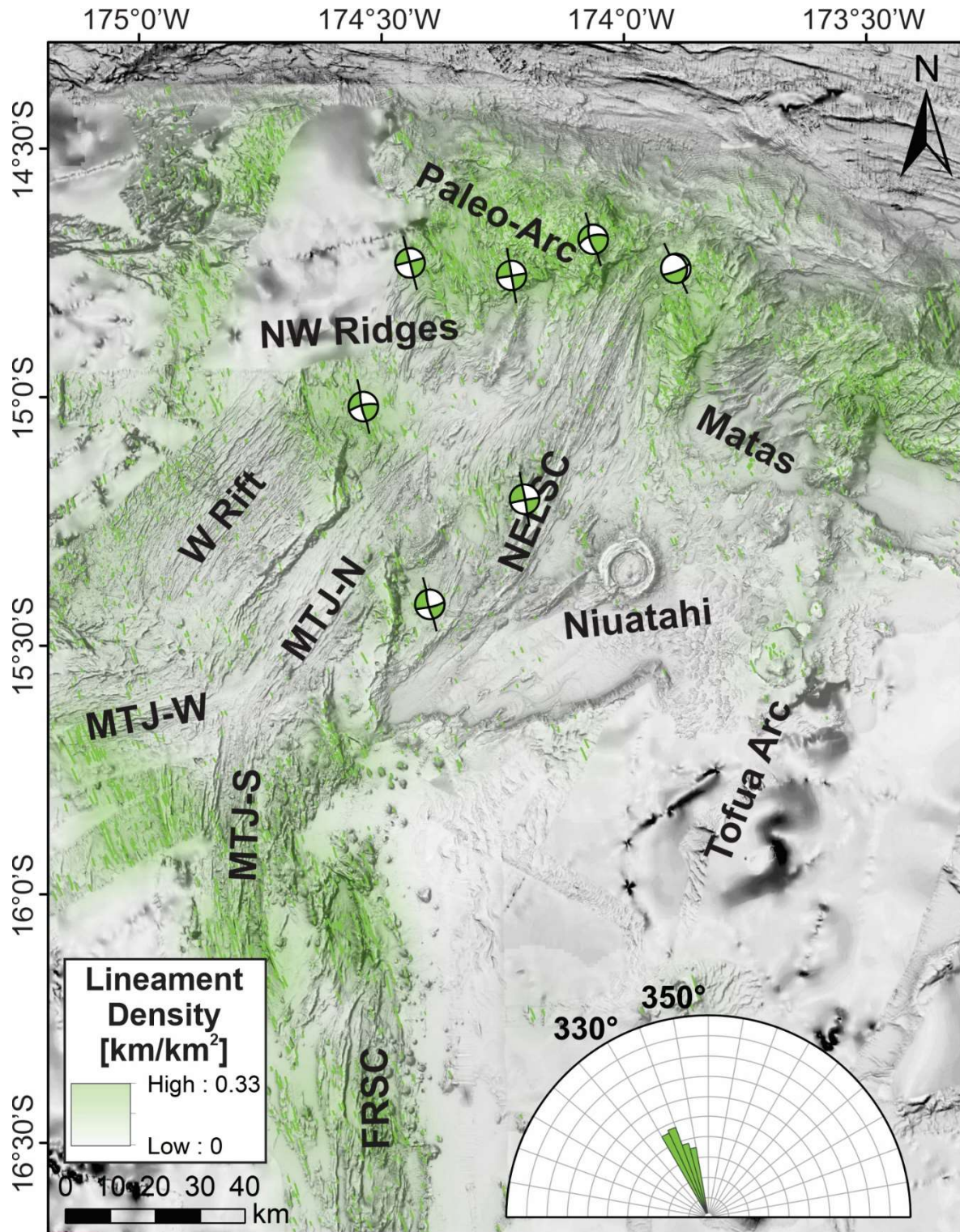


**Supplementary Figure S38.** Close-up of interpreted WNW-trending structural lineaments (**Fig. 7g**), relative lineament densities (km per km<sup>2</sup>) and shallow ( $\leq 25$  km) CMT focal plane solutions ([www.globalcmt.org](http://www.globalcmt.org); Dziewonski et al., 1981; Ekström et al., 2012). Abbreviations as in **Figure 2**.



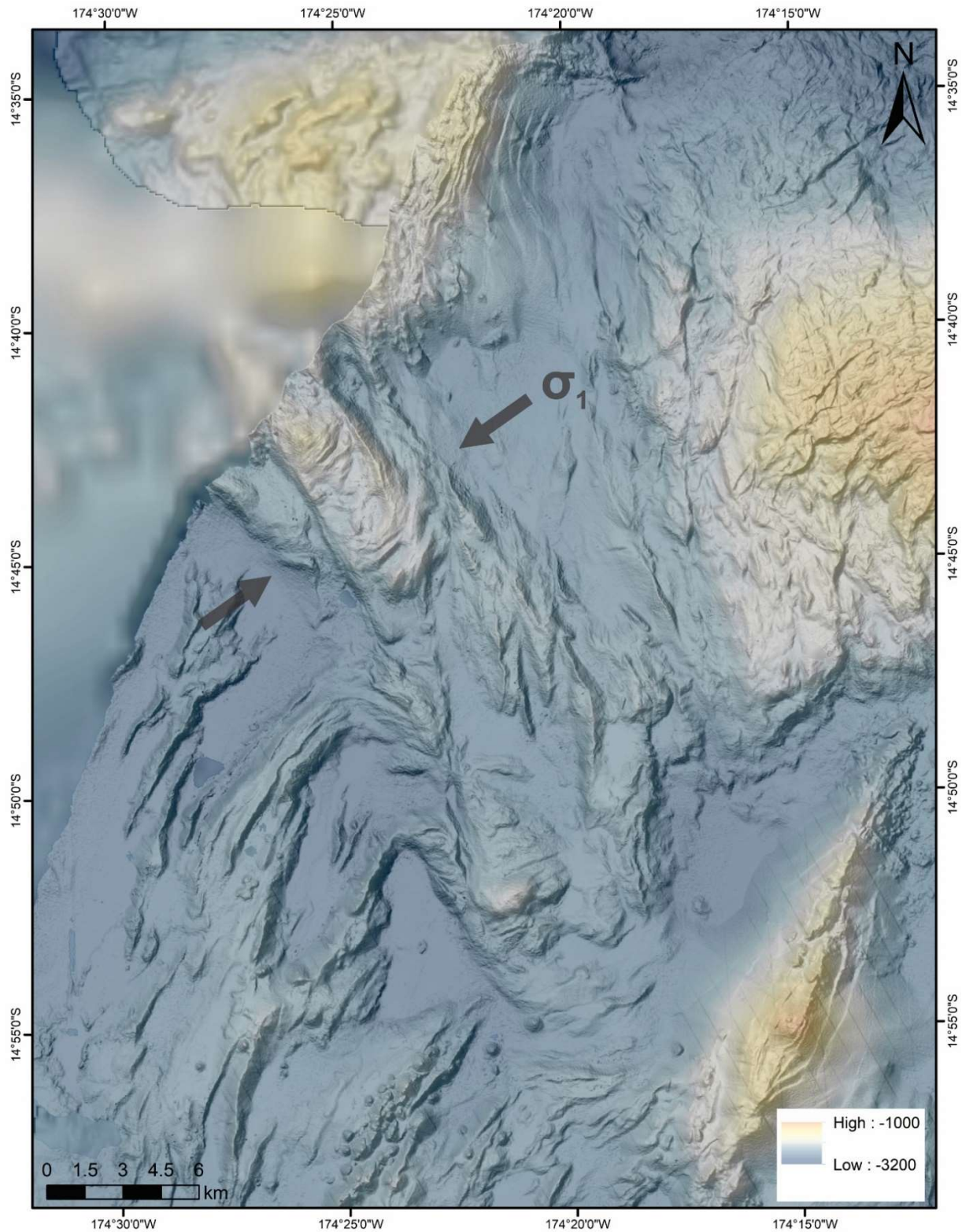


**Supplementary Figure S39.** Close-up of interpreted NW-trending structural lineaments (**Fig. 7h**) and relative lineament densities ( $\text{km per km}^2$ ). No shallow CMT focal plane solutions ( $\leq 25 \text{ km}$ ) were identified in this orientation. Abbreviations as in **Figure 2**.





**Supplementary Figure S40.** Close-up of interpreted NNW-trending structural lineaments (**Fig. 7i**), relative lineament densities (km per km<sup>2</sup>) and shallow ( $\leq 25$  km) CMT focal plane solutions ([www.globalcmt.org](http://www.globalcmt.org); Dziiewonski et al., 1981; Ekström et al., 2012). Abbreviations as in **Figure 2**.



**Supplementary Figure S41.** Close-up of the possible anticline feature within the NW Ridges assemblage, which may result from  $\sigma_1$  compression in the Riedels System 1 shown in **Figure 9**.



## 1.2 Supplementary Tables

**Supplementary Table S1.** Characteristics of crustal types shown in **Figure 4**

Crustal Type	Lithology <sup>1</sup>	Location	Inferred Age	Morphology	Vertical Gravity Gradient <sup>2</sup>	Seafloor Magnetization <sup>3</sup>	Multichannel Seismic Reflection <sup>4</sup>
<b>Lau back-arc crust</b>	Basalt with minor basaltic andesite	On the upper plate behind the volcanic arc	<4 Ma (Zellmer and Taylor, 2001; Taylor and Martinez, 2003)	Deepest parts of the seafloor characterized by numerous spreading centers, volcanic ridges, and small volcanic edifices, with normal faulting and small sedimented basins off-axis	Variable, following linear trends	Positive anomalies along spreading centers, variable off-axis	Sedimentary basins on back-arc crust, numerous normal faults
<b>Lau rear-arc crust</b>	Siliceous dacite and boninite	On the upper plate immediately behind the volcanic arc	<4 Ma (Zellmer and Taylor, 2001; Taylor and Martinez, 2003)	Characterized by large volcanic edifices (cratered and ridge-like volcanoes) surrounded by flat-lying crust with lava flows and/or sediment, with a notable absence of spreading centers or normal	Variable	Variable	N/A
<b>Tofua arc crust</b>	Basalt to basaltic andesite	Parallel to the trench on the upper plate, ~100 km above the subducting slab	<3.5 Ma (Tappin et al., 1994)	Large discrete volcanic edifices that are aligned along a front, topographically higher than surrounding crust, lacking faulting	Uniformly high along single linear trend	Mostly uniform positive anomalies along single linear trend	Flat-lying reflectors with high amplitude
<b>Paleo-arc crust</b>	Adakite, boninite, minor basalt and gabbro	Occurs immediately to the south of the STEP boundary and paleo Vitiaz trench	<12 Ma (Termination of subduction at Vitiaz trench: Ruellan et al., 2003; Ruellan and Lagabrielle, 2005)	Higher topographic relief relative to surrounding crust, intensely faulted/deformed	Uniformly high along single linear trend	Uniformly positive anomalies along single linear trend	N/A
<b>Pacific Plate crust</b>	Undifferentiated	Occurs to the north and east of the Tonga trench	<40 Ma (Oligocene to early Miocene: Meffre et al., 2012; Lagemaat et al., 2018)	Characterized by a deep trench and trench-parallel normal faults	Undifferentiated	Undifferentiated	N/A




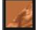




<sup>1</sup>As shown in Supplementary Fig. S3

<sup>2</sup>VGG from Sandwell et al. (2014)

<sup>3</sup>0.5-arc-minute magnetic data from Austin (2012) and references therein













<sup>4</sup>Extrapolated from FRSC survey by Schmid et al. (2020)

**Supplementary Table S2.** Description of the remote-predictive geological map units of the NE Lau Basin (**Fig. 5**) in order of generally increasing relative age

Assemblage	Unit Name	Description	Interpretations and Assumptions	Area [km <sup>2</sup> ]
<b>Clastic Cover Assemblage</b>				
	Volcaniclastic Sediment, Rippled	Smooth to rippled terrain with a wavy texture, cascading flows radiate out from arc volcanoes and submarine calderas.	Likely dominated by volcaniclastic material derived from the Tofua Arc volcanoes, including pumice and glass fragments.	16,484
	Pelagic/Volcaniclastic Sediment	Smooth terrain surrounding the other units, deposited in low-lying areas. Mostly featureless, very low backscatter in areas where	Likely a mixture of pelagic and volcaniclastic sediment.	3,860
<b>Tofua Arc Assemblage - Basalt to Basaltic Andesite</b>				
	Lava Flows	Areas of high backscatter near the northernmost arc volcanoes, including small flows within the graben that hosts the Niuua Volcanic Complex. Flows extend westward towards the dacitic Niuatahi Flows	Unsampled, likely basaltic andesite to andesite in composition similar to the proximal arc volcanoes. There may be considerable compositional changes between the small	214
	Niuua Volcanic Complex	Northernmost arc volcano with distinct rectangular gross morphology, up to 25 km long and 13 km wide, with numerous small overlapping cones and a strongly tectonized appearance.	Basaltic-andesite to andesite in composition; pumice sampled by Haase et al. (2018).	304
	Small Volcanic Edifices	Small, irregular topographic features that mainly occur to the west of the Tofua arc.	Not sampled, may be related to rear-arc volcanism.	293
	Large Volcanic Edifices	Flat-topped and conical stratovolcanoes that are dominantly submarine and decrease in size towards the northern termination of the arc. Many contain large caldera structures. Volcanoes K, L, Niuatoputapu are all apparently inactive. Curacoa erupted in 1979. Aligned along a chain that appears segmented and parallel to sub-parallel to the trench. Margins are covered by volcaniclastic sediment, outlined by inflection point in bathymetry (contacts uncertain)	Variable composition, mainly basaltic-andesite to andesite (Keller et al., 2008; Sleeper, 2017).	2,526
<b>Mata Rear-Arc Assemblage - Boninite</b>				
	Lava Flows	Areas of high-backscatter and low relief surrounding the Mata volcanoes, generally small in size.	Likely boninitic in origin, erupted from the Mata volcanoes.	61
	Volcanic Ridges	Area of nine en echelon volcanic ridges with variable orientations with both ridge-like morphologies and central point-source focused magmatism. These volcanoes have been actively erupting over the last 2 Ma, with older occurrences extending into the fore-arc region (Rubin and Embley, 2016; Chadwick et al., 2019). The southern volcanoes, West and East Mata, are 1400 to 1700 m tall. The northern Mata volcanoes are 900 to 1300 m tall.	Composed of boninitic pyroclastic material and lava flows (Resing et al., 2011b, Rubin and Embley, 2012).	473














**Supplementary Table S2.** Continued

Assemblage	Unit Name	Description	Interpretations and Assumptions	Area [km <sup>2</sup> ]
<b>Niauatahi Rear-Arc Assemblage - Dacite</b>				
	 Young Lava Flows	Young low-viscosity sheet flows with ropey surfaces, endogenous domes/ridges, inflated lobes, and collapse features (Embley and Rubin, 2018). Two of the largest flows flank the Niauatahi volcano, several smaller flows extend up to 60 km north of Niauatahi. Very high backscatter signatures.	Dacitic in composition, northern flows have a different composition than the flows surrounding Niauatahi (Embley and Rubin, 2018), not distinguished based on composition here.	481
	 Old Lava Flows	Slightly older low-viscosity sheet flows identified mainly by the backscatter signature, which is higher than the surrounding seafloor but lower than the young flows. Some flow morphologies still visible, but fine-scale features obscured.	Not sampled or distinguished by Embley and Rubin (2018), but likely dacitic in composition similar to the younger flows.	159
	 Constructional Volcanic Edifice(?)	Enigmatic low-relief mounds surrounded by dacitic flows, aligned along sub-linear trends, raised ~200 m above the surrounding seafloor. The morphology of the mounds is irregular, curved, and slightly hummocky.	Of interpreted volcanic origin, may be hummocky flows erupted along a fissure. Not sampled but likely dacitic in composition similar to the younger flows.	162
	 Niauatahi Caldera Volcano	Large, 15-km wide circular volcano with 8-km wide caldera with nested caldera structures. Caldera rim is breached in the north and south along a N-trending structure. Resurgent dome in the south-central area (Mototahi).	Dacitic submarine volcano of uncertain origin (Embley and Rubin, 2018), with a distinct morphology compared to other submarine calderas in the W Pacific (e.g., Kulo Lasi; Fouquet, 2018).	196
<b>FRSC Assemblage - Basalt to Basaltic Andesite</b>				
	 Neovolcanic Zone	Axial valleys with narrow axial volcanic ridges surrounded by smooth, featureless seafloor that may be sheet flows or volcanoclastic sediment (limited backscatter information).	Limited sampling in the study area, IAB affinities indistinguishable from the Tofua arc, with relatively homogenous composition along axis (Keller, 2008).	2, 836
	 Large Volcanic Ridges	Coalesced cones and a large volcanic ridge, 1350 m tall and 29 km long north of the northernmost FRSC segment.	Not sampled. Transitional from the old volcanic ridges, cones, and flows. Difficult to distinguish boundaries with MTJ assemblage.	659
	 Old Volcanic Ridges, Cones, Flows	Terraine outside of the axial valley, dominated by small volcanic cones and cone fields, coalescing into the large volcanic ridges.	Limited sampling suggests similar compositions to the neovolcanic zone (Keller, 2008). Difficult to distinguish boundaries with MTJ assemblage.	2,342
	 Faulted Old Crust	Steeply-dipping normal faults bounding the axial valleys over a narrow area.	Limited areal extent suggests low crustal stretching and/or young age of this spreading center.	660
<b>NELSC Assemblage - Basalt</b>				
	 Neovolcanic Zone	Flat-lying sheet and minor hummocky pillow flows in central axial valleys/ridges. High backscattered. Magmatically robust in the south.	Recently-erupted basalt (Haase et al., 2018) with an IAB signature and OIB mantle component (Niu and O'Hara, 2003; Zhang et al., 2018). Basaltic andesite at the northern tip are intermediate between MTJ lavas and enriched boninites (Falloon, 2007).	884
	 Large Volcanic Ridges	Large volcanic ridges up to 1260 m tall, with high backscatter due to high relief.	Limited sampling. Compositions are likely similar to the Neovolcanic Zone.	322
	 Old Volcanic Ridges, Cones, Flows	Symmetrical ridges and small cones, possible hummocky flows. Heavily sedimented with low backscatter.	Limited sampling. Compositions are likely similar to the Neovolcanic Zone. Ridges may be tilted fault blocks.	874
	 Faulted Old Crust	Normal inward-dipping fault scarps (high backscatter) parallel to the spreading axis, surrounded by flat-lying areas with low backscatter. Old fissure-style volcanism along some of these faults, lesser amounts of volcanic cones. Asymmetrical profiles.	Tilted fault blocks indicate relatively low crustal stretching (Kearey, 2009), with tilted fault blocks most evident along the northernmost extent.	428







**Supplementary Table S2.** Continued

Assemblage	Unit Name	Description	Interpretations and Assumptions	Area [km <sup>2</sup> ]
<b>MTJ Assemblage - Basalt to Basaltic Andesite</b>				
	 Neovolcanic Zone	Axial valley dominated by sheet flows and small fissures; northern and southern ends of the MTJ-N consist of small volcanic ridges up to ~180 m tall and the central portion of the segment has a broad morphology and subtle axial graben.	Mainly tholeiitic basalts on W and S arms, while the N arm is composed of basaltic andesites and andesites (Tian et al., 2011). MOB-like affinities similar to Lau BABB (Keller et al., 2008), transitional between N-MORB and IAB (Zhang et al., 2018). Minimal sampling along the MTJ-W.	1,196
	 Large Volcanic Ridges	Large volcanic ridge to the north of MTJ-N up to 1300 m tall and 17.5 km long; low-relief cratered volcanoes to the NW of the triple junction	Not sampled. The large volcanic ridge north of MTJ-N may instead be associated with the NELSC.	379
	 Old Volcanic Ridges, Cones, Flows	Narrow zone of volcanic ridges that parallels the spreading arms; the western extent along the MTJ-S is unknown due to poor-resolution bathymetry. Limited backscatter, mostly low.	Not sampled. Transition to the FRSC assemblage is unclear, likely gradational in area of overlap.	2,451
	 Faulted Old Crust	Narrow zone of inward-dipping normally-faulted terrane parallel to the spreading axis, with steep faults along the MTJ-N. Scarps are characterized by high backscatter.	Not sampled. The steep faults on the western side of MTJ-N transition into the steep escarpment (Escarpment Don Fig. 3).	1,193
<b>W Rift Assemblage - Unknown (Basalt?)</b>				
	 Lava Flows	Dominated by sheet flows that mostly cover pre-existing faulted fabric, with abundant collapse features. Volcanic activity is most abundant to the west of the map area near the subaerial Niuafóu volcanic island. High backscatter area. These flows are also interpreted to the north of Escarpment C (Fig. 3), but the transition to the NW Ridge assemblage is uncertain.	Unsampled, likely basaltic based on proximity to MTJ. Composition may be similar to the Niuafóu volcano.	1,678
	 Old Volcanic Ridges, Cones, Flows	Mainly WNW- and NW-trending volcanic ridges that cross-cut the dominant NE-fabric of this area. This unit is interpreted to extend to the NE towards the paleo-arc crust, but interpretations are limited by poor-resolution bathymetry.	Unsampled, likely basaltic based on proximity to MTJ.	1,064
	 Faulted Old Crust	Sub-vertical fault scarps parallel to the MTJ-N, dipping inwards towards a central graben. Little volcanism, abundant sedimentation in low-lying areas revealed by low backscatter. Zig-zag faults and intersecting faults common.	Unsampled, likely basaltic based on proximity to MTJ.	1,317
<b>NW Ridges Assemblage - Unknown (Basalt?)</b>				
	 Volcanic Ridges	Volcanic ridges with variable orientations, mainly linear features that are sub-parallel to the NELSC. Individual ridges rise to heights of 760 m above the surrounding seafloor. Surrounding areas are interpreted to be sediment, although backscatter data is lacking in this area.	Unsampled, likely basaltic. May reflect distal portion of the NELSC.	553
<b>Back-Arc Crust</b>				
	 Faulted Old Crust (Boninite?)	Back-arc crust exposed in large escarpments that rise over 1 km from the surrounding seafloor.	Composition unknown, likely reflecting the oldest back-arc material in the map area. Escarpment A (Fig. 3) sampled by Haase et al. (2018).	617
	 Core Complex(?)	Possible core complex along Escarpment C (Fig. 3) characterized by corrugated surface perpendicular to a large escarpment. Interpretation is uncertain due to lack of seafloor observations or sampling.	Unsampled, composition uncertain.	30
	 Undifferentiated Crust	Areas where ship multibeam bathymetry is lacking, no discernable/identifiable features.	Unsampled, composition and origin uncertain.	6,059



## Supplementary Table S2. Continued

Assemblage	Unit Name	Description	Interpretations and Assumptions	Area [km <sup>2</sup> ]
<b>Paleo-Arc Assemblage - Adakite, Boninite, Basalt</b>				
	 Volcanic Cones and Ridges(?)	Areas of paleo-arc crust that appear to be small volcanic ridges and cones with a relatively youthful morphology, although backscatter data is lacking. This may be where volcanism is captured from the back-arc near the NW Ridge Assemblage and the Mata Assemblage.	Unsampled, composition and origin uncertain.	682
	 Faulted Old Crust	Blocky, heavily tectonized crust with a bulging gross morphology, interpreted to be paleo-arc crust formed when the Pacific Plate was actively subducting beneath the Vitiaz Trench. Backscatter data is	Limited sampling, variable composition ranging from basalt to andesite to adakite (Falloon et al., 1987) and boninite (Haase et al., 2018). Unit includes paleo-forearc material as well.	205
	 Displaced Faulted Old Crust	Blocky crust, similar in appearance to the Faulted Old Crust, but located distal to the Vitiaz Trench. Backscatter data is lacking.	Unsampled, likely similar composition to the Faulted Old Crust. Interpreted to be crustal block that was displaced during the opening of the NELSC.	9,548
<b>Pacific Plate Assemblage</b>				
	 Undifferentiated Crust	Pacific Plate crust, including Samoan seamounts. Characterized by trench-parallel normal faults associated with bending of the down-	Undifferentiated.	4,956